

**Department of Physics and Astronomy  
University of Heidelberg**

Bachelor Thesis in Physics  
submitted by

**Jens Petersen,**

born in Hamburg (Germany), on

**30th of April, 2013**



# **Performance Analysis of a Transceiver Chipset and Interference Control for a Wireless Detector Readout at 60GHz**

This Bachelor Thesis has been carried out by Jens Petersen at the  
Institute of Physics (Physikalisches Institut) in Heidelberg  
under the supervision of  
Prof. Dr. André Schöning

## ABSTRACT

The high luminosity upgrade of the Large Hadron Collider (LHC) will increase the event rate in the ATLAS detector by a factor of 10. To be able to better resolve an increasing number of pile-up events, the inclusion of tracking detector information in first level trigger decisions is necessary. After the silicon micro-strip tracker upgrade in 2022, this would require an overall readout bandwidth between 50 and 100 Tb/s. A wireless readout with radial line-of-sight readout links using the license-free 60 GHz frequency band offers capacity up to 10 Gbps per link. It could be connected to on-detector trigger logic to reduce latency, which would make a level 1 track trigger with the ATLAS silicon strip tracker upgrade feasible. At the same time, the technology would put little strain on both power and material budget.

As 60 GHz radiation is reflected completely by silicon, which is found in the tracker, cross-talk would likely be an issue. An approach to suppressing cross-talk and multipath interference with ultra-light materials will be presented in this work. To evaluate the 60 GHz ASICs under development, a reliable testbench is necessary. In this work, the performance of a commercial transceiver evaluation kit using IQ baseband modulation is investigated. Technical challenges such as clock distribution and phase stability are addressed.

## ZUSAMMENFASSUNG

Mit dem High Luminosity Upgrade des Large Hadron Collider (LHC) wird sich die Event-Rate im ATLAS-Detektor um den Faktor 10 erhöhen. Um die zunehmende Anzahl von Pile-Up Ereignissen besser auflösen zu können, ist es nötig, Informationen vom Track-Detektor in die unterste Trigger-Entscheidung mit einzubeziehen. Nach dem für 2022 geplanten Upgrade des Silicon Micro-Strip Trackers würde das eine Auslese-Bandbreite von 50 bis 100 Tb/s erfordern. Eine kabellose Auslese mit radial orientierten und auf Sichtausbreitung beschränkten Links im lizenzenfreien 60 GHz-Band bietet bis zu 10 Gbps Kapazität pro Link. Die Auslese-Elektronik könnte mit Triggerlogik innerhalb des Detektors kombiniert werden, um die Trigger-Latenz zu reduzieren, und so einen L1 Track Trigger mit dem Silicon Strip Tracker Upgrade für ATLAS möglich machen. Außerdem würde die Technologie das Leistungs- und Massebudget wenig belasten.

60 GHz-Strahlung wird von Silizium, welches sich im Track-Detektor findet, vollständig reflektiert, weshalb Cross-Talk eine Schwierigkeit darstellen kann. Ein Ansatz, diesen mit ultraleichten Materialien zu unterdrücken, wird in dieser Arbeit präsentiert. Um zukünftige 60 GHz-ASICs testen zu können, ist ein verlässliches Referenzsystem notwendig. In dieser Arbeit wird die Performance eines kommerziellen Transceiver Evaluation Kit untersucht, welches IQ-Basisband-Modulation verwendet. Technische Herausforderungen wie Clock-Verteilung und Phasenstabilität werden erörtert.

# CONTENTS

<b>1. Introduction</b>	<b>1</b>
1.1. The ATLAS Detector . . . . .	1
1.2. L1 Track Trigger . . . . .	3
1.3. The WR15 Frequency Band . . . . .	3
<b>2. Transmission Stability</b>	<b>4</b>
2.1. Methods & Instrumentation . . . . .	4
2.1.1. Bit Error Rates . . . . .	4
2.1.2. High Bandwidth Transceiver Chipset . . . . .	5
2.1.3. Full Transceiver Evaluation Kit . . . . .	5
2.1.4. Modulation Schemes . . . . .	6
2.1.5. Signal Integrity & Eye Diagrams . . . . .	8
2.2. Observations and Measurements . . . . .	9
2.2.1. Bit Error Rate Measurements . . . . .	9
2.2.2. FPGA Signal Quality . . . . .	9
2.2.3. Phase Instability . . . . .	11
2.2.4. Stable Transmission with the High Bandwidth Transceiver Chipset	13
2.2.5. Transmission Spectrum . . . . .	14
<b>3. Graphite Foam Absorber</b>	<b>17</b>
3.1. Methods & Setup . . . . .	18
3.2. Measurements & Results . . . . .	20
<b>4. Kapton Foil Gain Horn</b>	<b>24</b>
4.1. Experimental Setup . . . . .	25
4.2. Measurements & Results . . . . .	26
<b>5. Discussion</b>	<b>31</b>
<b>References</b>	<b>34</b>
<b>A. Appendix</b>	<b>36</b>

# 1. INTRODUCTION

Future particle detection experiments, especially multi-purpose ones like ATLAS, will often be required to handle a much larger collision rate than today. An example is the high luminosity LHC upgrade that aims for a tenfold increase of 14 TeV pp-collisions compared to the current LHC performance [1]. High event rates not only produce more data that need to be processed, but also more pile-up, which can be resolved by high granularity detectors like the ATLAS silicon strip tracker that again produce more data. Brenner and Cheng [2] describe how millimeter wave technology, especially in the 60 GHz frequency band, could be used to wirelessly read out detector data and to include tracking detector information for a fast first level trigger decision. A first prototype for an ASIC using *On-Off Keying (OOK)* and offering data rates up to 3.5 Gbps is being developed by Soltveit et al. [3], who also see data rates of 10 Gbps at a first level track trigger with the ATLAS silicon strip detector feasible.

Apart from the high bandwidth a wireless readout potentially offers a number of other advantages. Among these are the easier assembly and disassembly of the detector, low material budget and little power consumption [2]. However, extremely high radiation hardness would be required from the technology. Cross-talk and multipath interference are a challenge suggesting the use of ultra light antennas with high directivity and absorbers.

This work aims to analyze the performance of a full commercial transceiver evaluation kit that could potentially be used as a reference system for future ASICs specifically designed for a 60 GHz detector readout. Furthermore, the absorption and reflection characteristics of graphite foam as well as the beam forming performance of aluminized Kapton foil are investigated to see if these materials, which offer a low atomic number and low density/thickness to prevent multiple scattering and hadronic interactions, could serve to eliminate the cross-talk issue.

## 1.1. THE ATLAS DETECTOR

The ATLAS detector, seen in fig. 1.1, is one the four big multi-purpose experiments at the *Large Hadron Collider (LHC)* at CERN. The silicon strip detector (semiconductor tracker) is part of the inner detector, displayed in fig. 1.2, which also features a pixel detector and a transition radiation detector. It currently faces an event rate of about  $10^9$  Hz, which is reduced to a much smaller number by a 3 level trigger system. The first level hardware trigger has a reduction factor of 400 and a decision latency of  $2.5\ \mu\text{s}$  [4] and is followed by two software trigger levels that reduce the data to a final rate of 200 Hz of events that are stored and analyzed. Each event is equivalent to 1.6 MB of raw data after the third level trigger [5]. Inner detector data are read out parallel to the detectors cylindrical axis, hence numerous cables run within the detector and can potentially cause multiple scattering. In contrast, the wireless readout discussed in this work would be radial, reducing the probability of unwanted interactions.

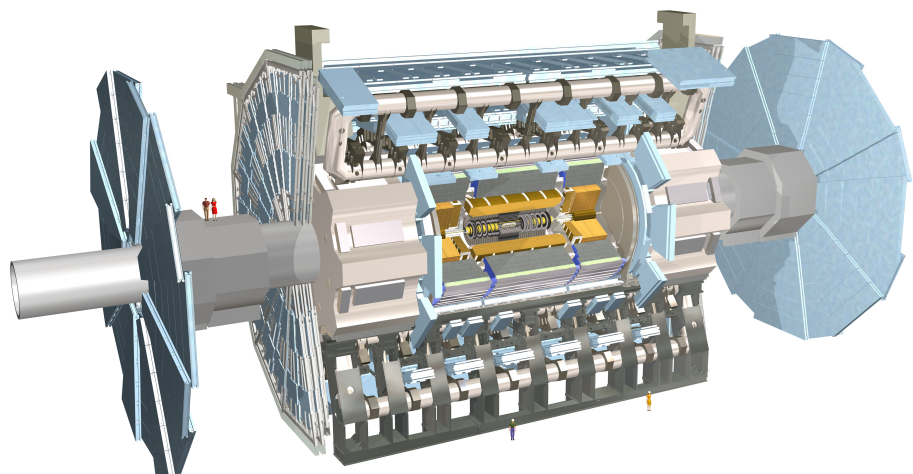


Figure 1.1.: A model of the ATLAS detector [5]

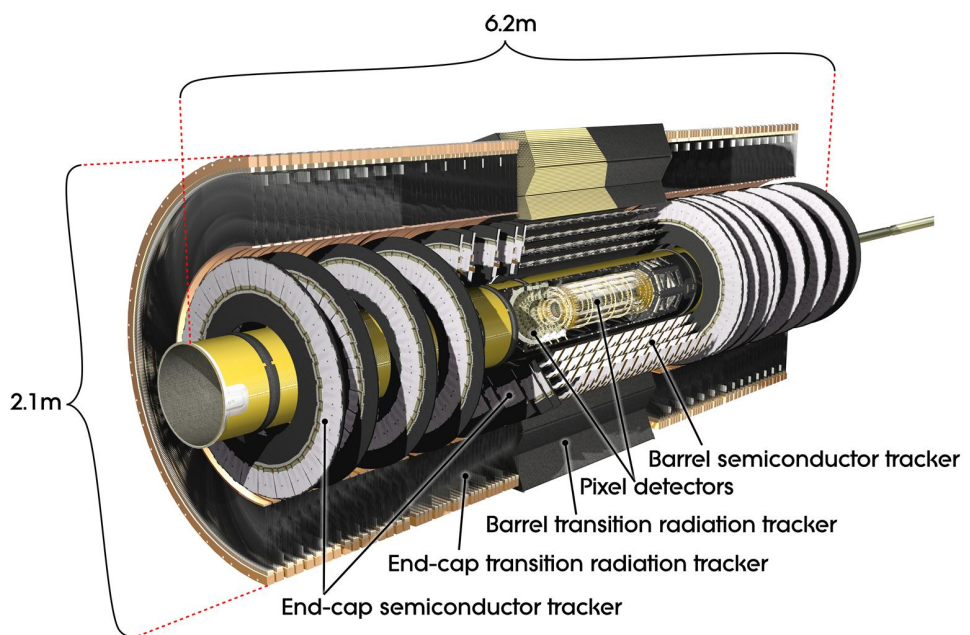


Figure 1.2.: Inner detectors of the ATLAS experiment [5]

## 1.2. L1 TRACK TRIGGER

A level one (L1) track trigger would include information of a tracking detector for trigger decisions on the lowest level. This could be implemented with the ATLAS silicon microstrip tracker upgrade, which is planned for 2022 [6]. The high granularity of tracking detectors is useful to discriminate particles in pile-up events but also demands a high bandwidth. The latter is offered by 60 GHz technology. As the upgraded ATLAS tracking detector will produce up to 100 Tb/s of data [2], each link will have to transmit about 5 Gbps [2]. In addition to allowing for the required data rates, a wireless radial readout in combination with on-detector decision logic could reduce the latency of the L1 trigger compared to the current situation [3], where first level data are processed close to but outside the detector and need to travel several tens of meters and one meter equals  $\sim 3.3$  ns delay.

## 1.3. THE WR15 FREQUENCY BAND

The acronym WR15 denotes the license-free frequency band around 60 GHz. The unlicensed spectrum is defined differently depending on the region, ranging from 3.5 GHz bandwidth in Australia to 7 GHz in most other regions. In Europe it's defined from 59 GHz to 66 GHz, as seen in fig. 1.3. The wavelength corresponding to 60 GHz is roughly 5 mm, hence technology in this domain is often referred to as millimeter wave technology.

The free-space path loss of 60 GHz radiation is 68 dB/m [7], limiting the use to short range applications that include near-field radar, communications technology such as Wireless HD [8] or spectroscopy and diagnostic applications [7].

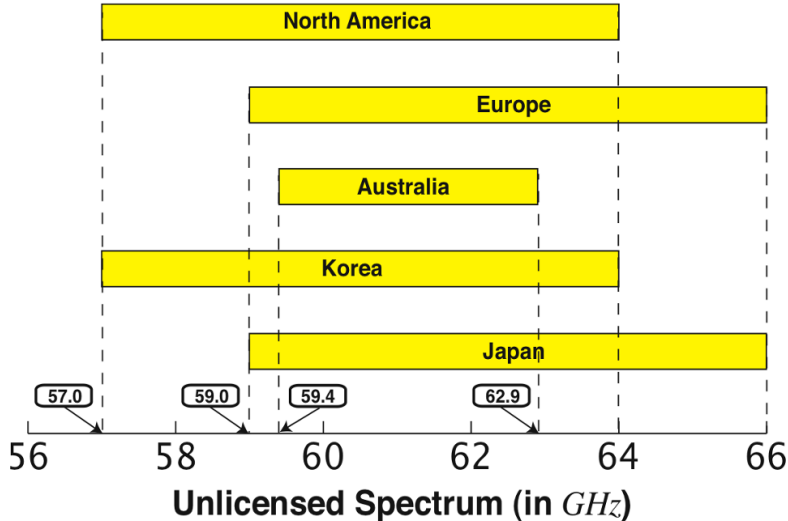


Figure 1.3.: The WR15 band: License-free spectrum for different regions [2]

## 2. ANALYSIS OF TRANSMISSION STABILITY

The aim of this work was to set up a wireless reference system and to establish a reliable testbench for future systems. It was possible to uphold stable transmission over periods of  $\sim 10$  s, allowing to estimate bit error rates. In order to test the reference system and to identify causes of transmission instabilities, several technical aspects are addressed. Although two transceiver chipsets were at disposal, all measurements except the ones in section 2.2.4 were performed with the more advanced transceiver chipset introduced in section 2.1.3.

### 2.1. METHODS & INSTRUMENTATION

#### 2.1.1. BIT ERROR RATES

The data used to determine the bit error rate (BER) were pseudo-random, meaning that they don't have a narrow frequency spectrum like for example alternating ones and zeros, hence look random, but are reproducible. There are numerous ways of how pseudo-random data can be created, one of which are *Linear Feedback Shift Registers (LFSR)*. Figure 2.1 illustrates a Fibonacci method LFSR that generates a bit by applying a row of XOR operations. The created pseudo-random bit is then placed at the first position of the bit string and all other bits are shifted to the next position. The process is then repeated and the complete random bit sequence can be reproduced when the starting bit vector is known [9].

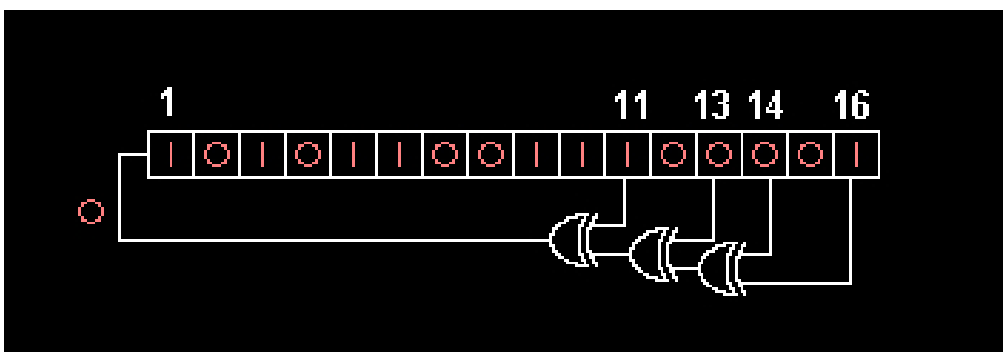


Figure 2.1.: Schematic of a 16-bit Linear Feedback Shift register using the Fibonacci method (Public domain picture taken from Wikipedia)

In this experiment, the data were created using a programmable device/FPGA on a commercial board (from Altera<sup>1</sup>). After passing through the complete transmission cycle, i.e. transmitter stage, wireless transmission and receiver stage, they were analyzed with the same FPGA and the BER was determined. Due to problems, which will be discussed in detail in section 2.2.1, stable transmission was only possible for very short time spans, about ten seconds. This time was insufficient for exact measurements. Instead, a rough estimate of the order of the BER is given.

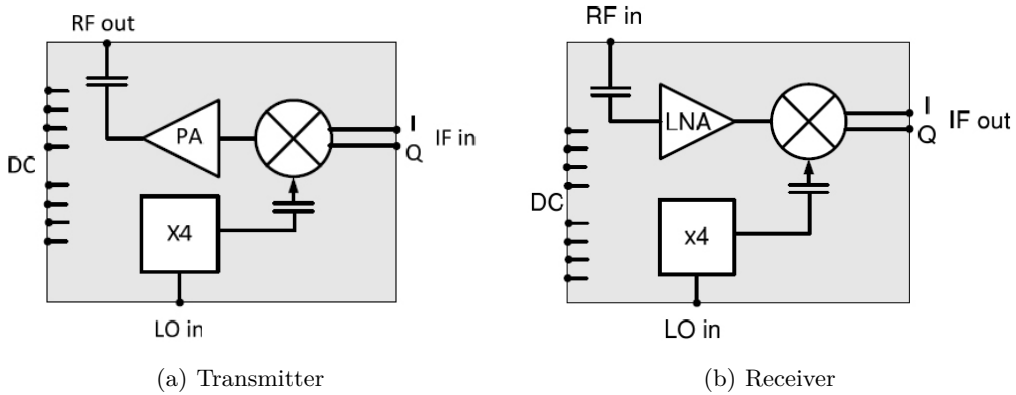


Figure 2.2.: Gotmic transmitter and receiver layout [10][11]

### 2.1.2. HIGH BANDWIDTH TRANSCEIVER CHIPSET

One of two transceiver chipsets used for the experiments that are presented in this work was provided by Gotmic<sup>2</sup>, namely TXQ060A01 [10] and RXQ060A01 [11]. The chips include a  $\times 4$  multiplier stage, a power amplifier and an IQ modulator/demodulator, as seen in fig. 2.2. Supply voltages for the chips need to be provided externally, enabling control of all the stages' bias settings, which is necessary for a comprehensive analysis of the chips' functionality. The chipset was provided on a testboard with a waveguide coupling output. Transmitter inputs and receiver outputs were non-differential. The IF bandwidth of the chipset was 8 GHz [10].

A brief presentation of the chips' performance in transmitting lower frequency (1 MHz to 200 MHz) sinusoidal signals will be given in section 2.2.4.

### 2.1.3. FULL TRANSCEIVER EVALUATION KIT

For all measurements except the ones presented in section 2.2.4 a commercial transceiver set from Hittite<sup>3</sup> was used. The transmitter and receiver chips were HMC6000 [12] and HMC6001 [13], respectively. The chips came with a board featuring a USB connector that could be used to set the carrier frequency, attenuation and amplification. Every time new settings were transferred, the clock circuitry was reset, which turned out to be of importance, as described in section 2.2.3. Voltages were derived internally from a single power supply, so that it was not possible to analyse single stages for possible malfunction. Two identical boards both comprising a transmitter and a receiver chip were at disposal. Unless otherwise stated, only a single board was used for the experiments. Each module

<sup>1</sup>[www.altera.com](http://www.altera.com)

<sup>2</sup>[www.gotmic.se](http://www.gotmic.se)

<sup>3</sup>[www.hittite.com](http://www.hittite.com)

offered 8 inputs, 4 of which were dedicated to the use of MSK (see section 2.1.4). The 4 others were the I input and the Q input, both differential. The receiver featured the corresponding 4 outputs.

It was possible to choose between two internal quartz oscillators at roughly 285 MHz and 308 MHz or an external clock of 308 MHz. The influence of the clocks on the RF spectrum and hence the transmission quality will be presented in section 2.2.5. The IF bandwidth of the transmitter was specified as 1.8 GHz, which would theoretically allow data rates up to 3.6 Gbps. However, it was found that for rates  $> 1.8$  Gbps the signal was attenuated considerably with highly increased rise and fall times. It was therefore decided to only use rates up to 1.6 Gbps for the experiments.

In contrast to the Gotmic products, the RF signal output and input was facilitated by an MMPX connector, from which the signal could be distributed to a waveguide using appropriate cables and adapters. A schematic of the chips' layout is given in figs. A.1 and A.2.

#### 2.1.4. MODULATION SCHEMES

As the frequency band around 60 GHz offers a lot of bandwidth (see section 1.3), it is possible to employ a simple modulation scheme such as *On-Off Keying (OOK)* or *Frequency Shift Keying (FSK)*, offering less spectral efficiency (transmitted data per frequency) than a more sophisticated method but guaranteeing a higher transmission stability. An overview over the most common modulation methods including their performance can be found in Freeman [14]. The transceiver used in this experiment and introduced in section 2.1.3 allows for two modulation techniques, simple baseband IQ modulation and *Minimum Shift Keying (MSK)*. The latter was not used, as it required additional instrumentation not available at the time of carrying out this work. A detailed presentation of MSK can be found in Pasupathy [15].

##### Baseband IQ modulation

In IQ modulation the transmitted signal  $s(t)$  is constructed from two independent inputs  $I(t)$  and  $Q(t)$  multiplied with two sinusoid signals offset by  $90^\circ$ :

$$s(t) = I(t) \cdot \cos(\omega_c t) - Q(t) \cdot \sin(\omega_c t) \quad (2.1)$$

with the carrier frequency  $\omega_c$ , for example  $\omega_c = 2\pi \cdot 60\text{GHz}$ . The received signal  $r(t)$  will in general contain errors  $e(t)$  in addition to the sent signal as a result of other emitters' signals being picked up by the receiver as well.

$$r(t) = s(t) + e(t) \quad (2.2)$$

The original input can be found by multiplying  $r(t)$  with the same sinusoidal as on the transmitter side. In the ideal case ( $e(t) = 0$ ) [16]:

$$\begin{aligned} I_r(t) &= r(t) \cdot \cos(\omega_c t) = s(t) \cdot \cos(\omega_c t) \\ &= I(t) \cdot \cos^2(\omega_c t) - Q(t) \cdot \sin(\omega_c t) \cos(\omega_c t) \\ &= \frac{1}{2} I(t) + \frac{1}{2} [I(t) \cdot \cos(2\omega_c t) - Q(t) \cdot \sin(2\omega_c t)] \end{aligned} \quad (2.3)$$

$$Q_r(t) = \frac{1}{2} Q(t) - \frac{1}{2} [I(t) \cdot \sin(2\omega_c t) + Q(t) \cdot \cos(2\omega_c t)] \quad (2.4)$$

The high frequency content can be filtered out by a low pass. The demodulation must be coherent, meaning that it requires the transmitter and the receiver sinusoids to be in phase. This modulation technique just reproduces, ideally that is, the two independent input signals. Thus it leaves room for further modulation as for example in quantized *Quadrature Amplitude Modulation (QAM)*, which uses the amplitude of the two signals and their relative phase to encode data [17].

There are numerous parameters in which reality deviates from the ideal case. Small distortions can have a potentially big influence on the received signal. The results presented in section 2.2 demand an in-depth discussion of those influences, hence now a detailed presentation of different error sources other than the additive error of eq. (2.2).

### Frequency instability

Transmitter and receiver are fed by the same external clock, so small distortions thereof should have the same effect on both entities, leaving the received signal unaltered. However, it might be possible that circuitry imperfections and other factors lead to a small frequency difference between transmitter and receiver. Assuming that  $s(t)$  is created with  $\omega_c$  but the demodulation is performed with  $\omega_c + \Omega(t)$ , with  $\Omega$  being small in comparison to  $\omega_c$ , the situation changes as follows:

$$\begin{aligned} s(t) &= I(t) \cdot \cos(\omega_c t) - Q(t) \cdot \sin(\omega_c t) \\ I_r(t) &= s(t) \cdot \cos(\omega_c t + \Omega t) \\ &= I(t) \cdot \cos(\omega_c t) \cos(\omega_c t + \Omega t) - Q(t) \cdot \sin(\omega_c t) \cos(\omega_c t + \Omega t) \\ &= I(t) \cdot \cos^2(\omega_c t) - I(t) \cdot \Omega t \cdot \sin(\omega_c t) \cos(\omega_c t) \\ &\quad - Q(t) \cdot \sin(\omega_c t) \cos(\omega_c t) + Q(t) \cdot \Omega t \cdot \sin^2(\omega_c t) \\ &= \frac{1}{2} I(t) + \frac{1}{2} Q(t) \cdot \Omega(t) \cdot t \end{aligned} \tag{2.5}$$

$$Q_r(t) = \frac{1}{2} Q(t) - \frac{1}{2} I(t) \cdot \Omega(t) \cdot t \tag{2.6}$$

using Taylor approximation and ignoring high frequency content. This is of course only a valid approximation if  $\Omega t$  is sufficiently small in comparison to  $\omega_c t$ , but it shows that the error component increases over time. For a constant  $\Omega \neq 0$  an oscillation between  $I(t)$  and  $Q(t)$  would occur on either output.

### Phase instability between transmitter and receiver

It is likely that the clock for the transmitter and for the receiver are not completely in phase. For a phase difference  $\phi(t)$  between the modules, again using Taylor approximation and neglecting high frequency content, the received signals will have the following form:

$$\begin{aligned} s(t) &= I(t) \cdot \cos(\omega_c t) - Q(t) \cdot \sin(\omega_c t) \\ I_r(t) &= s(t) \cdot \cos(\omega_c t + \phi) \\ &= \frac{1}{2} I(t) + \frac{1}{2} Q(t) \cdot \phi(t) \end{aligned} \tag{2.7}$$

$$Q_r(t) = \frac{1}{2} Q(t) - \frac{1}{2} I(t) \cdot \phi(t) \tag{2.8}$$

The need for a coherent demodulation is clearly visible. The influence can only be neglected for small  $\phi(t)$ .

### Phase instability between I and Q

The carrier sinusoids are ideally offset by  $90^\circ$ . Deviations from that can occur on both the transmitter and the receiver side,  $\alpha_T(t)$  and  $\alpha_R(t)$  respectively:

$$\begin{aligned} s(t) &= I(t) \cdot \cos(\omega_c t) - Q(t) \cdot \sin(\omega_c t + \alpha_T) \\ I_r(t) &= s(t) \cdot \cos(\omega_c t) \\ &= \frac{1}{2}I(t) - \frac{1}{2}Q(t) \cdot \alpha_T(t) \end{aligned} \tag{2.9}$$

$$\begin{aligned} Q_r(t) &= s(t) (-\sin(\omega_c t + \alpha_R)) \\ &= \frac{1}{2}Q(t) \cdot [1 + \alpha_T(t)\alpha_R(t)] - \frac{1}{2}I(t) \cdot \alpha_R(t) \end{aligned} \tag{2.10}$$

Again it is assumed that errors are small enough for Taylor approximation and high frequency content is neglected.

#### 2.1.5. SIGNAL INTEGRITY & EYE DIAGRAMS

To provide a better understanding of the actual shape of the signal and the changes it undergoes during transmission, eye-diagrams both before and after transmission were recorded and will be compared. These diagrams comprise a large number of overlayed signal samples equally triggered, yielding a pictogram that often resembles an array of eyes that indicates how well the logic states 1 and 0 are separated and for how long. From these graphs a number of key parameters describing the signal quality can be extracted easily, such as rise- and fall-time, jitter or eye-width and -height. The results will be compared to those of the BER measurements.

## 2.2. OBSERVATIONS AND MEASUREMENTS

### 2.2.1. BIT ERROR RATE MEASUREMENTS

As mentioned before, stable transmission was only possible for approximately ten seconds, stable meaning that the measured BER was reasonably low. The reason for this is most likely found in the signal distortion observed in section 2.2.3. Within this time span, almost no bit errors occurred and error rates  $< 10^{-11}$  were recorded for the highest data rate 1600 Mbps. For lower data rates the BER limits were a little higher, simply because less data could be transmitted in the given time. For 400 Mbps error rates  $< 10^{-9}$  could be achieved. Other data rates between 400 Mbps and 1600 Mbps returned error rate limits between  $10^{-9}$  and  $10^{-11}$ .

When waiting longer, error rates quickly jumped to  $10^{-6}$  and then rose to around  $10^{-3}$ , where they remained fairly stable. This was tested with a 12-hour run at 800 Mbps. Each period of stable transmission was followed by roughly 1.5 min of high error rates before a reset could yield low rates again. The desired outcome would of course be that no reset at all is necessary to achieve low BER.

### 2.2.2. FPGA SIGNAL QUALITY

To give an idea of the quality of the signal used for measurements in this section, a selection of eye diagrams at different data rates is given in fig. 2.3. The internal standard was the Altera proprietary PCML [18] on a differential SMA output, connected to the board via a mezzanine card [19]. To give a more quantitative description of the signal, some key parameters are listed in table 2.1. The ideal eye width is the inverse data rate.

Data Rate (ideal)	Data Rate (measured)	Eye Width (ideal)	Eye Width (measured)	Signal-to-Noise Ratio
800 Mbps	800.51 Mbps	1250 ps	1220.44 ps	47.17
1200 Mbps	1196.30 Mbps	833.3 ps	809.34 ps	27.68
1600 Mbps	1592.30 Mbps	625 ps	597.33 ps	23.12
2000 Mbps	1985.64 Mbps	500 ps	470.65 ps	18.93
3200 Mbps	3173.12 Mbps	312.5 ps	273.71 ps	14.72
4800 Mbps	4751.48 Mbps	208.33 ps	166.51 ps	12.30
6400 Mbps	6698.02 Mbps	156.25 ps	105.12 ps	8.72

Table 2.1.: FPGA output signal integrity parameters

For 800 Mbps the signal is of superior quality, with good SNR and close to an ideal eye, i.e. rectangular, only with a softer slope when approaching maximum amplitude, as seen in fig. 2.3(a). With increasing rates, the SNR drops significantly and the measured eye width becomes increasingly smaller than the ideal value, indicating a rise in both jitter and general signal fluctuation. While flawless communication is easily imaginable for 800 Mbps, a much higher error rate can be expected for 6400 Mbps. In this experiment 1600 Mbps was the maximum rate, so it is reasonable to assume that the input signal is not an error source for the issues presented in this chapter.

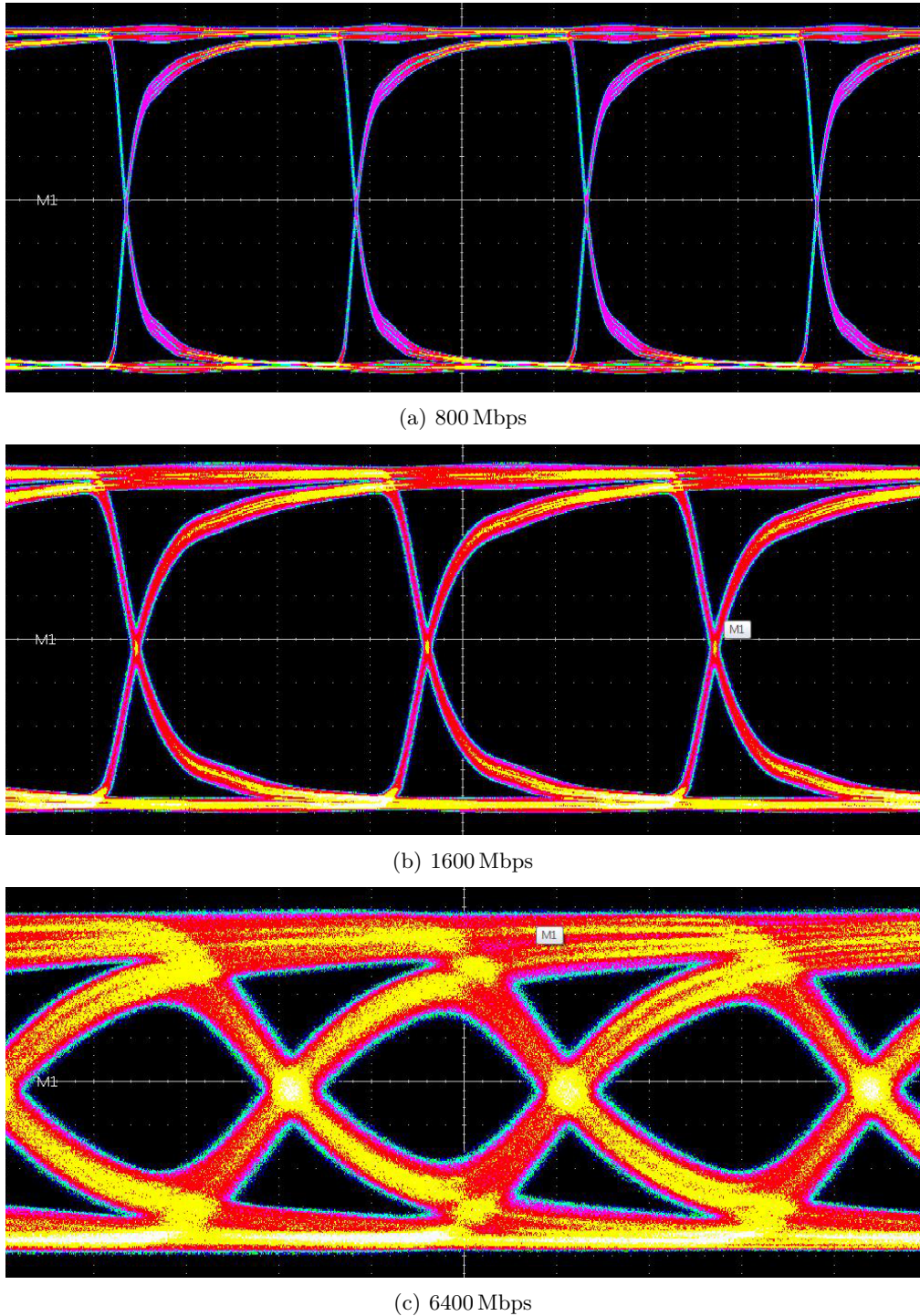


Figure 2.3.: FPGA output signal eye diagrams

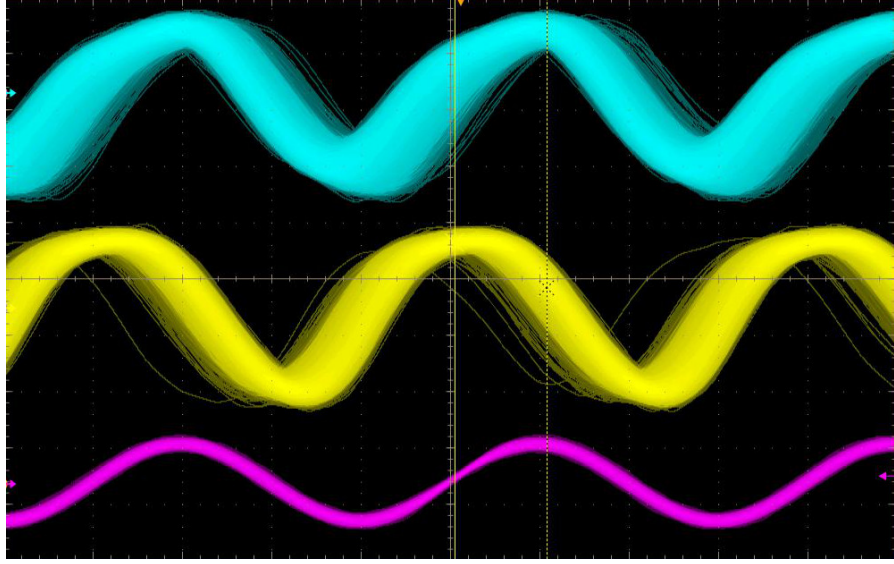


Figure 2.4.: Phasing of I output (yellow) and Q output (blue) relative to a 1 GHz sine on the I input (pink); 1 of 16 possible combinations

### 2.2.3. PHASE INSTABILITY

Feeding a signal only to the I input of the transceiver while leaving the Q input open should theoretically return the signal only on the I output, as seen in eqs. (2.3) and (2.4). This was not observed. Instead, both outputs returned the I input signal. The exact design of the modulation/demodulation circuitry was not available, but it's reasonable to assume this behaviour was intended by the manufacturer. Using the Q input gave the same results.

However, the relative phase of the two outputs as well as their phase referenced to the input, in this case a sinusoidal signal, showed unexpected behaviour. Every time the transmitter or the receiver was reset, which should ideally only be necessary to change the carrier frequency or other settings, the phase of the outputs randomly changed to a multiple of  $90^\circ$  with respect to the input, seemingly independent of each other. Of the 16 possible combinations, those with a  $90^\circ$  difference between the outputs occurred somewhat more often, but this was not tested sufficiently to assure statistical significance. The phase between input and output was not stable, but drifted over time. An example situation can be seen in fig. 2.4.

When either of the entities is reset, phase locked loops in its circuitry will set to the current phase of the input clock. As receiver and transmitter could not be locked at the same time, a random constant phase between the two will establish with every reset. Given that the loops only lock to certain phases of the clock, for example maximum amplitude and zero-crossing, the random multiple of  $90^\circ$  could be explained. The described behaviour was observed with a 1 GHz sine signal. A test with 150 MHz gave different results. The phase of the outputs did not change with a reset of the transceiver, but both outputs were heavily unstable in phase by up to  $\pm 70^\circ$ . The reason for this difference might be that the arbitrary set to a certain point of the clock input is like sampling the clock signal and that 150 MHz is not enough to completely "see" the phase difference, contrary to 1 GHz, which is more than twice the clock frequency.

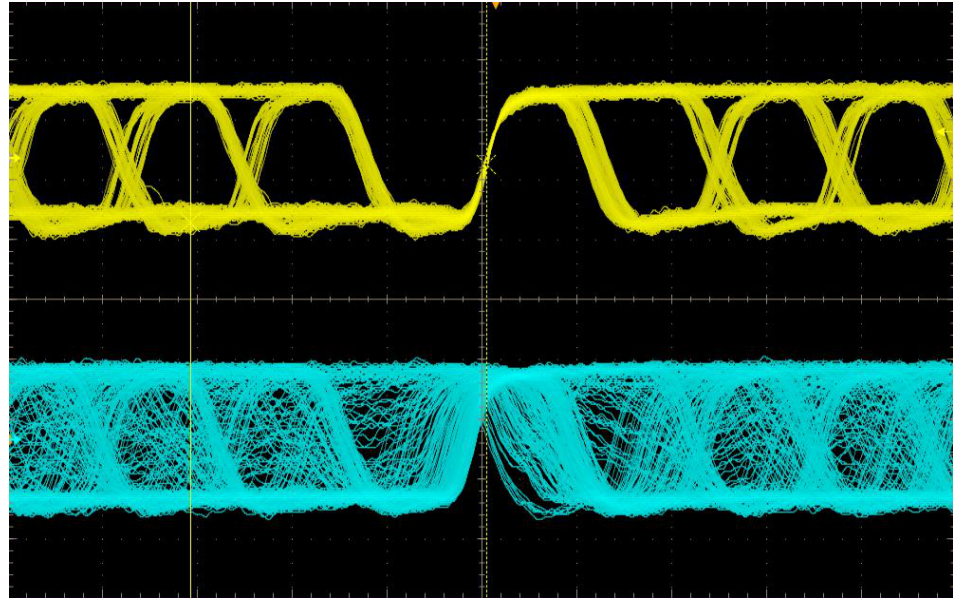


Figure 2.5.: I output (yellow) and Q output (blue) for a 800 Mbps bit signal on I; stable I output for a few seconds

While for sines the signal shape was unchanged by the transmission, bit pattern signals - which are of course what will eventually be transmitted in a detector readout, if no other modulation scheme is used - were often overlain by heavy distortion after transmission in contrast to before, as seen in section 2.2.2. At certain times one of the outputs returned a stable pattern, while the other presented said distortion. This situation is depicted in fig. 2.5. When waiting longer, both outputs would feature distortions, as seen in fig. 2.6.

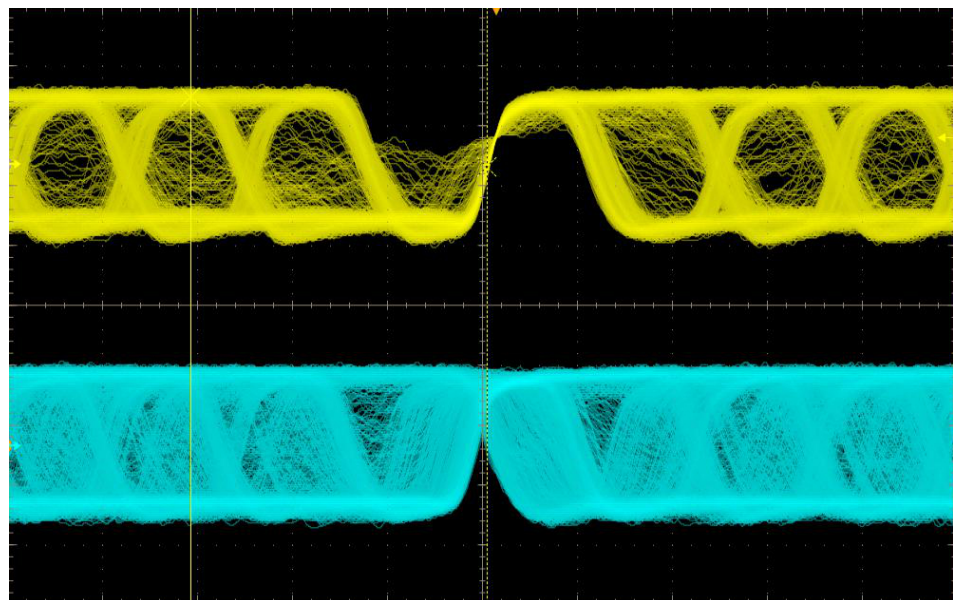


Figure 2.6.: I output (yellow) and Q output (blue) for a 800 Mbps bit signal on I; both outputs unstable

Over time, a periodic behaviour with a time constant of about 1.5 min could be observed, indicating a direct correlation with the bit error rate described in section 2.2.1. One output stabilized while the other was heavily distorted. It then started to present the same distortions increasingly often until both outputs did so equally. After that the other output started to stabilize until the described process repeated itself. This also happened when using the Q input instead of I or putting the signal on both inputs. Comparing fig. 2.5 with fig. 2.3(a), the change in signal shape for data signals can be seen. Most apparent is the increased rise and fall time, evident through the smaller slope. Considering that the signal passes numerous power amplifiers, the result is unsurprising. The distortion could indicate that the phase between transmitter and receiver wasn't locked, but internal feedback at some point in the circuitry, caused for example by signal amplitudes exceeding the specifications, could also be a reason. Input signals were of cause within the range specified in the documentation, but it would have been helpful to be able to measure voltages and currents for separate stages of the chips'. It might be useful to refrain from transmitting data signals directly, because rectangular shapes equal high frequency content, and instead use additional modulation that can convert data to lower frequency signals, for example MSK [15].

#### 2.2.4. STABLE TRANSMISSION WITH THE HIGH BANDWIDTH TRANSCEIVER CHIPSET

The Gotmic transceiver chipset in use had a very basic and straightforward design, as illustrated in fig. 2.2. Especially advantageous was the possibility of supplying all voltages externally, thus making them available for fine tuning. After fixing some issues revealed by testing the power consumption of the chips it was possible to establish transmission over a 12 mm distance directly from pad-antenna to pad-antenna without employing gain horns. Figure 2.7 shows the transmission of 50 MHz sinusoidal signal over the I channel. The receiver output has changed significantly in comparison to the input, looking like a sine with the upper half "cut off". That is likely a saturation effect, meaning that the power of the transmitted signal was too high.

In contrast to the Hittite transceiver modules, no phase instability other than some jitter was observed with the Gotmic set. However, this is not represented in fig. 2.7 and was only verified for frequencies  $< 200$  MHz. It would have been possible to conduct more experiments with this chipset, for example transmission of higher frequency signals, but only the transceiver evaluation kit by Hittite (see section 2.1.3) will potentially serve as a reference for other systems, so it was decided to discontinue measurements with the Gotmic chipset at an earlier stage of this work.

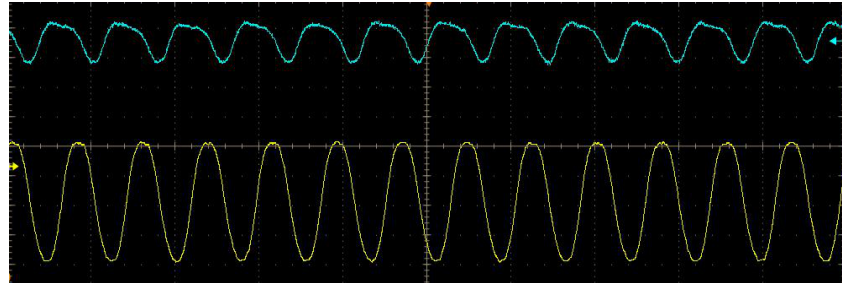


Figure 2.7.: Transmitting a 50 MHz sinusoid from pad-antenna to pad-antenna using the Gotmic transceiver chipset, input is yellow, output is blue

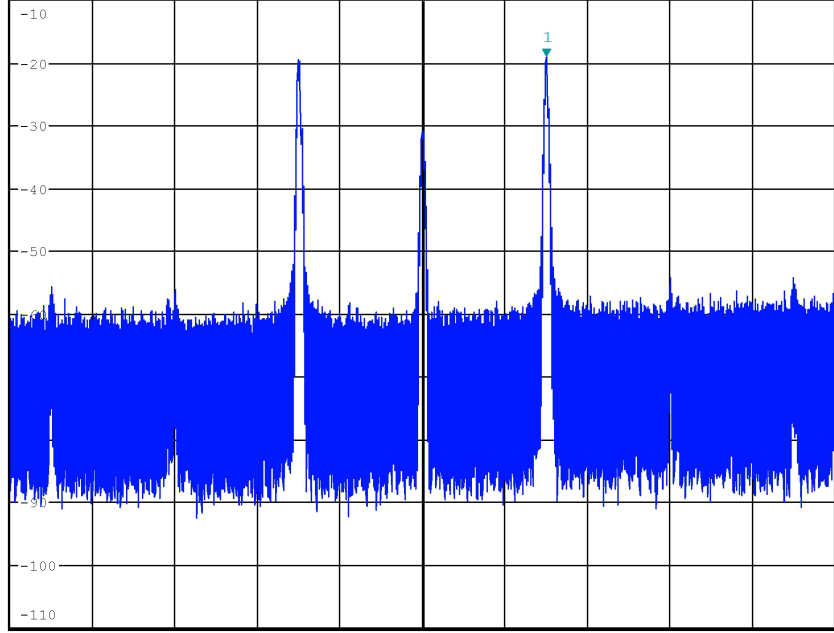


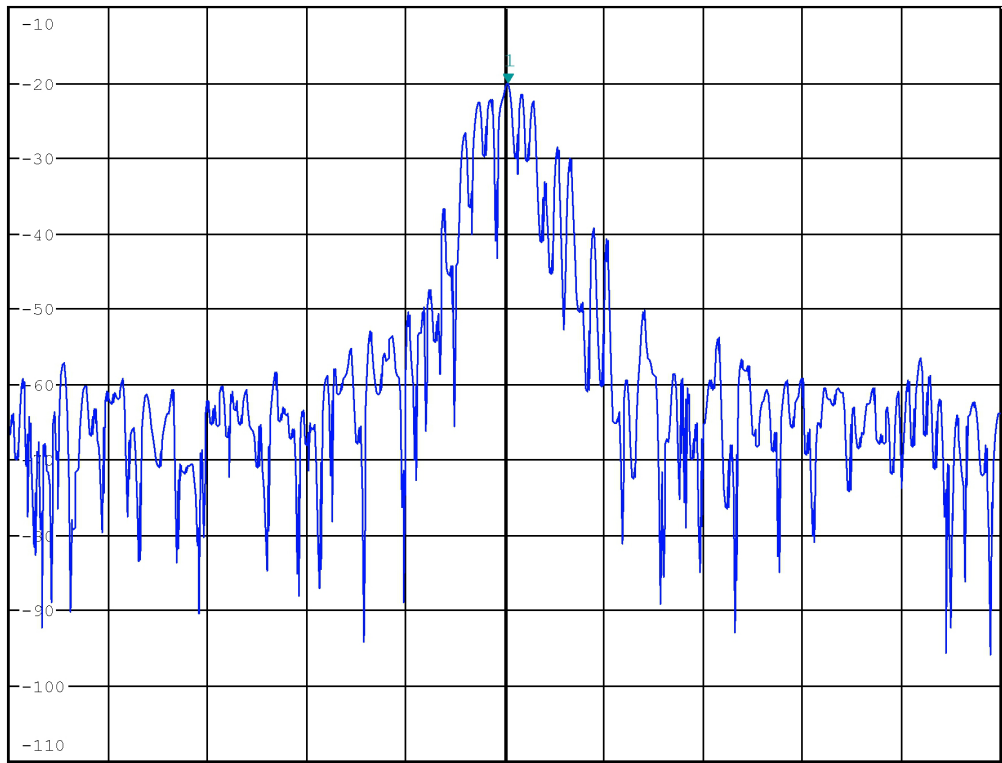
Figure 2.8.: Transmission spectrum for a 150 MHz sinusoid with 60.368 GHz (centered); 1 GHz span

### 2.2.5. TRANSMISSION SPECTRUM

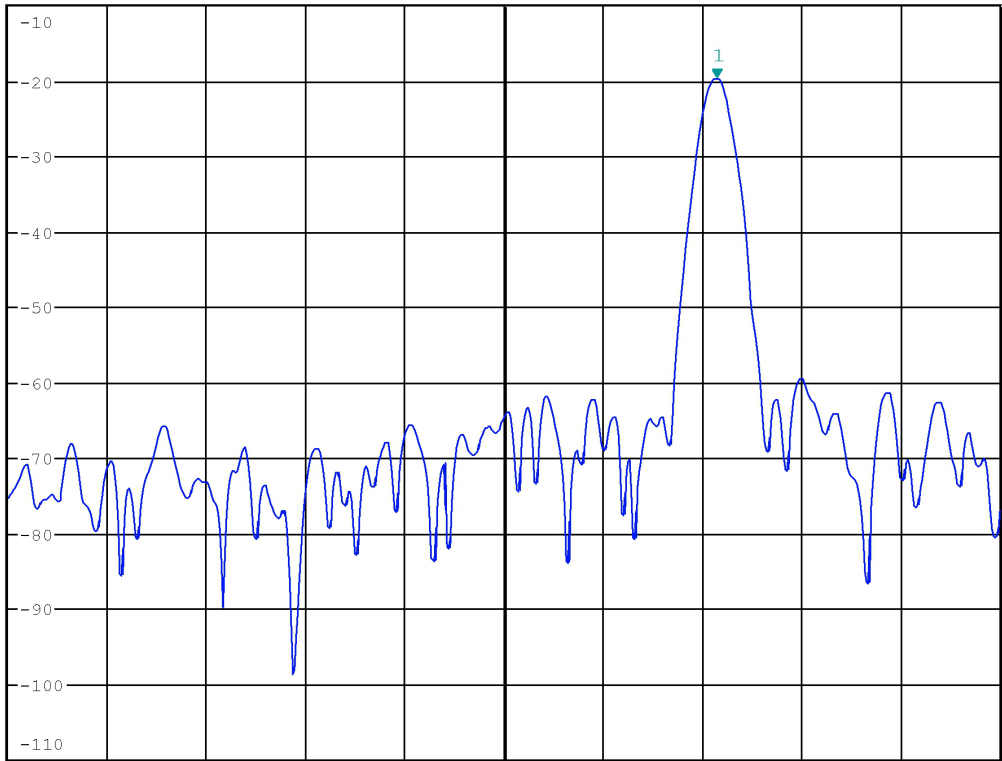
In section 2.1.4 it was shown that frequency stability is crucial for IQ demodulation. When supplying a sinusoidal signal of frequency  $\omega$  to one of the inputs, the spectrum around the carrier frequency  $\omega_c$  should consist of two peaks at  $\omega_c + \omega$  and  $\omega_c - \omega$ . In reality, the carrier frequency itself will also be visible as well as some other sidebands at distances of  $n \cdot \omega$  from the carrier, usually with much smaller intensity. The structure for the transmission of a 150 MHz sine can be seen in fig. 2.8.

With a span of 1 GHz no difference between the spectra for an external clock and for an internal clock could be observed, hence only the spectrum with external clock is presented in fig. 2.8. However, zooming in on the first upper sideband the difference is clearly visible. Figure 2.9(a) shows a 200 kHz range around the first upper sideband when using an external clock of 308.5714 MHz, which was the internal oscillator's frequency specified in the documentation. An arch of frequency peaks instead of just one peak is found, indicating a poor quality of the modulation.

For an internal clock of the same frequency, on the other hand, the peak shape was of superior quality, a discrete frequency peak with small width. This can be seen in fig. 2.9(b). However, the peak position was unstable and drifted within a 10 kHz range due to the instability of the internal quartz oscillator or an instability of the PLL, making a clean demodulation difficult. It was possible to achieve a similar quality with an external clock by fine tuning it, but the optimum adjustments depended on the input signal, hence had to be repeated for every new setup. The peak quality however was only good for a couple of seconds before an arch of frequencies, or at least a combination of multiple peaks, formed that again lasted for a couple of seconds. This process periodically repeated itself approximately every 20 s. Two examples are given in fig. 2.10. The distortion of the frequency peak was usually much stronger than in fig. 2.10(b). There is a likelihood that the unstable clock supply could have caused the other problems described before.

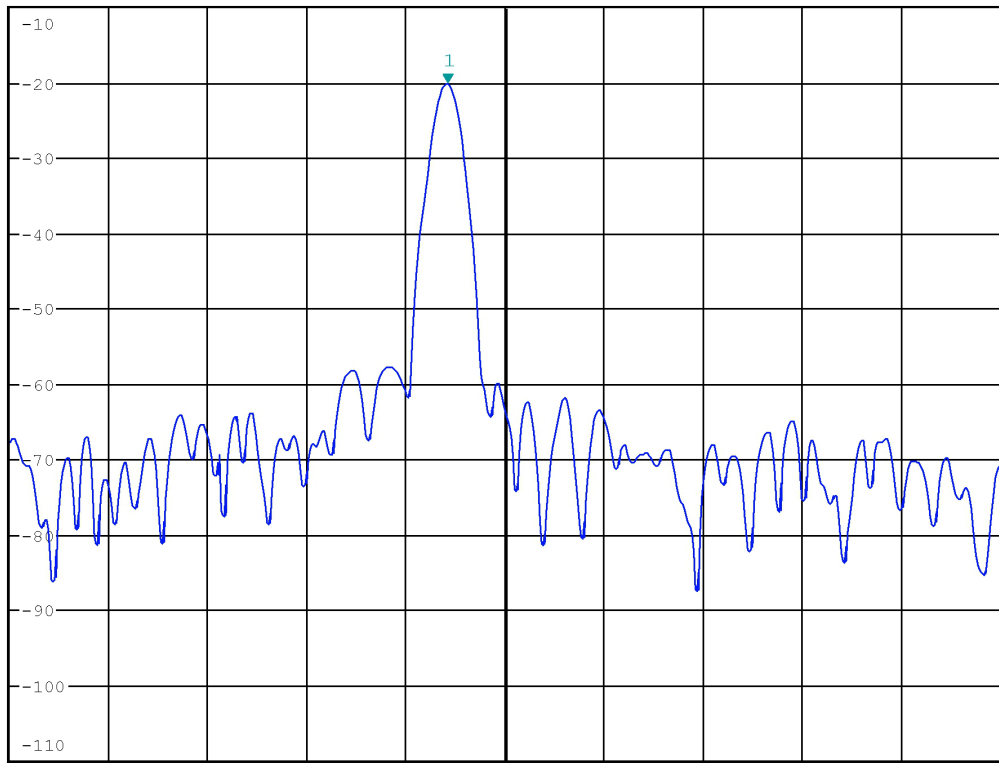


(a) First upper sideband transmitting a 150 MHz sine signal using an external clock of 308.5714 MHz; 200 kHz span

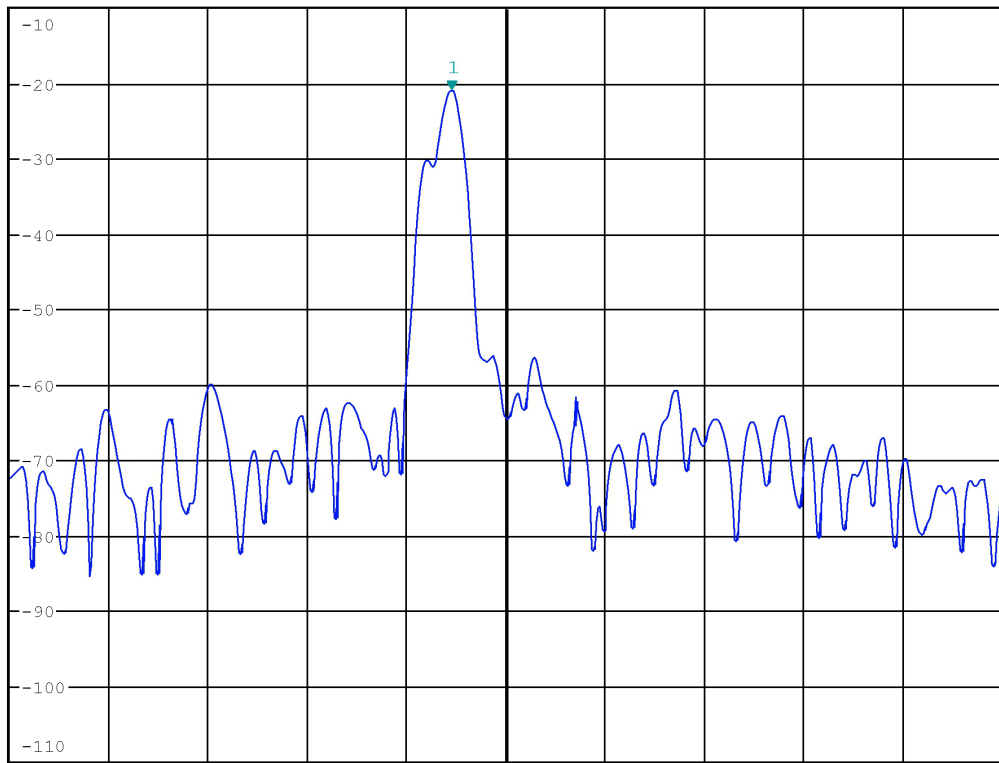


(b) First upper sideband transmitting a 150 MHz sine signal using an internal clock of  $(308.571 \pm 0.005)$  MHz; 10 kHz span

Figure 2.9.: External and internal clock of same frequency



(a) Optimized external clock, single peak



(b) Optimized external clock, distorted peak

Figure 2.10.: First upper sideband transmitting a 150 MHz sinusoid using an optimized external clock; 10 kHz span

### 3. GRAPHITE FOAM ABSORBER

A densely populated parallel and radial wireless detector readout as illustrated in fig. 3.1 makes it imperative to suppress sideways radiation in order to avoid cross-talk between links. That can be facilitated by a material highly absorbent for radiation in the order of 60 GHz, placed between the links (A in fig. 3.2) to reduce the intensity of reflected radiation or as a direct shielding of both transmitters and receivers (B in fig. 3.2), increasing the directivity of the links, or possibly both. A simulation of the latter was performed by Hugle [20]. Following up on the work of Felbecker et al. [21], graphite foam was analyzed in matters of absorbance, reflectivity and transmissivity, because it offers low density ( $32 \text{ kg/m}^3$  [22]) and low atomic mass (mainly  $12 \text{ u}$  for carbon).

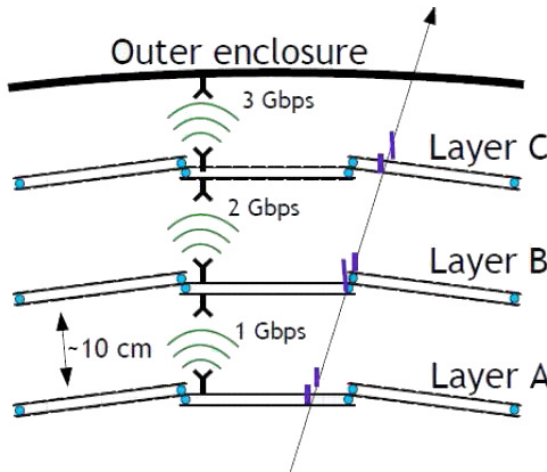


Figure 3.1.: Schematic of wireless radial detector readout [3]

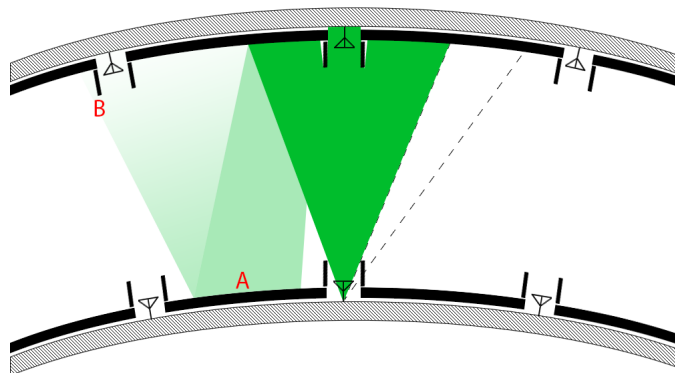


Figure 3.2.: Schematic of the radiation for wireless readout links; A - foam between links; B - foam shielding for antennas



Figure 3.3.: Close up of the analyzed graphite foam

### 3.1. METHODS & SETUP

The reflectivity of the material, a close up picture of which can be seen in fig. 3.3, was determined using two gain horns, one fixed and one mounted onto a rotating breadboard, so that the electromagnetic wave is incident on the foam under the angle  $\phi$ , while the receiving antenna is positioned at  $2\phi$  relative to the optical path. The setup is illustrated in fig. 3.4. To calculate the reflectivity of the material, the maximum intensity was measured with no material in the optical path and with  $\phi = 0$ . In addition to that, the intensity transmitted directly from antenna to antenna, not via reflections,  $I_{direct}$  was measured for every angle without reflecting material. The reflectivity was then

$$R(\nu, \phi) = \frac{I_r(\nu, \phi) - I_{direct}(\nu, \phi)}{I_{max}(\nu)} \quad (3.1)$$

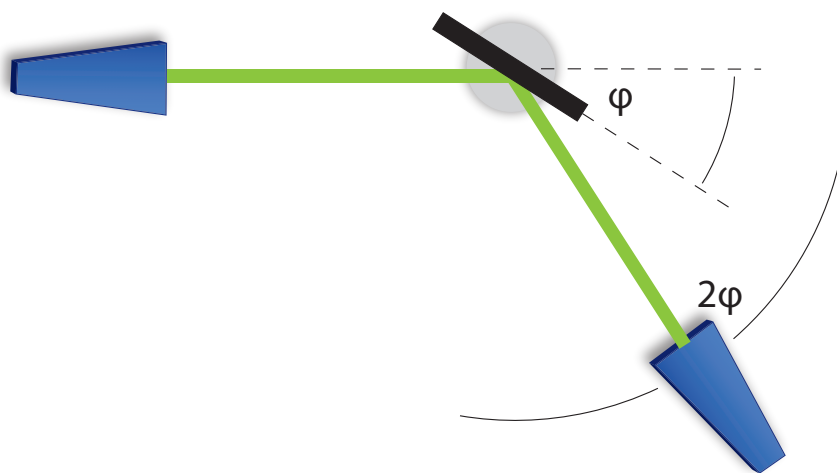


Figure 3.4.: Measuring the angular dependence of the reflectivity

To determine the absorption coefficient  $\alpha$  of the graphite foam the transmitted intensity was measured varying the thickness  $d$ . The antennas were placed directly onto both sides of the material, while the maximum transmission  $I_{max}$  was found removing all material from the path, as before with the reflectivity measurements, and approximating  $T \approx 1$  for air over very short distances (this approximation is inappropriate for longer distances, because oxygen molecules strongly absorb 60 GHz radiation [23]). Using the relation

$$T(\nu, d) = \frac{I_t(\nu, d)}{I_{t,max}(\nu, d)} \quad (3.2)$$

the attenuation coefficient could be found via the Lambert-Beer-Law [24]:

$$T(\nu, d) = A \cdot e^{-\alpha(\nu) \cdot d} + c \quad (3.3)$$

$A$  and  $c$  are additional parameters to correct for reflection losses. While eq. (3.3) might not necessarily describe the true nature of the process, because it requires  $d \gg \lambda$ , it does so sufficiently to estimate the absorptivity, as will be seen in section 3.2. The findings will be used to discuss possible benefits and disadvantages as well as the feasibility of using graphite foam to suppress cross-talk when reading out a detector with wireless links.

## 3.2. MEASUREMENTS & RESULTS

Several types of graphite foam, varying in their characteristics, were at disposal. To give an idea of their performance, the attenuation of one and the reflectivity of another were investigated.

Figure 3.5 shows the reflectivity of the foam with model number ML-10048-3 from ARC Technologies<sup>1</sup> for different frequencies. The incident angle is the angle between the optical path and the plane itself rather than its normal vector. The analyzed angular spectrum was geometrically limited.

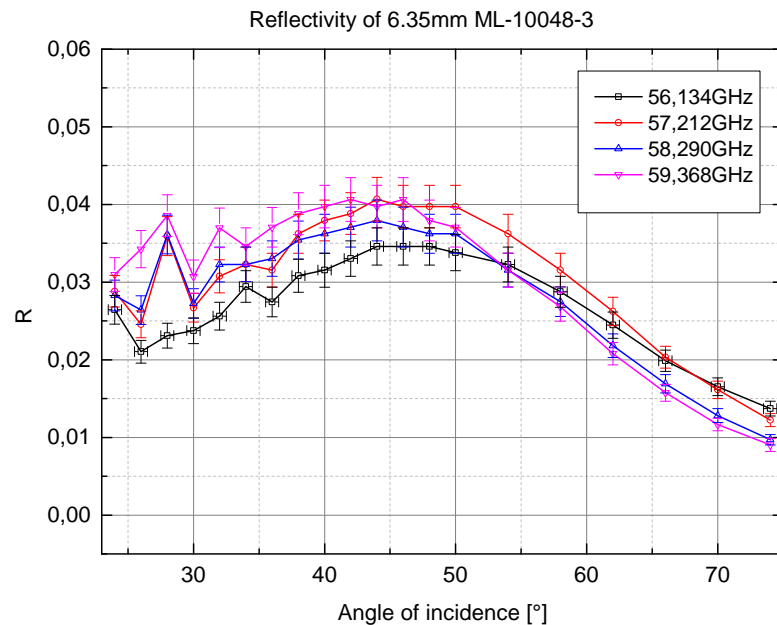
Between 50° and 75° the reflectivity decreases with increasing angle of incidence ( $\phi$ , as described in section 3.1 and fig. 3.4), as is to be expected from the Fresnel equations for flat surfaces. Flatness is a valid assumption since the foam's structural dimensions are well below the wavelength of the radiation. An elaborate discussion of the underlying principles can be found in Hecht [25]. The decrease seems to be slightly stronger for higher frequencies. Around 45° the reflectivity is highest and for smaller angles it decreases again fluctuating strongly. This behaviour is likely due to interference. While part of the radiation is reflected on the surface, another portion will be reflected on the back side of the foam. For certain angles constructive or destructive interference can take place. The wavelength of 60 GHz radiation is roughly 5 mm. As the piece was 6.35 mm thick, constructive interference would be observed around 58°, 39°, 31°, 25°, ... following Bragg's Law [26]

$$(\phi_{max})_n = \arcsin\left(\frac{2d}{n\lambda}\right) \quad (3.4)$$

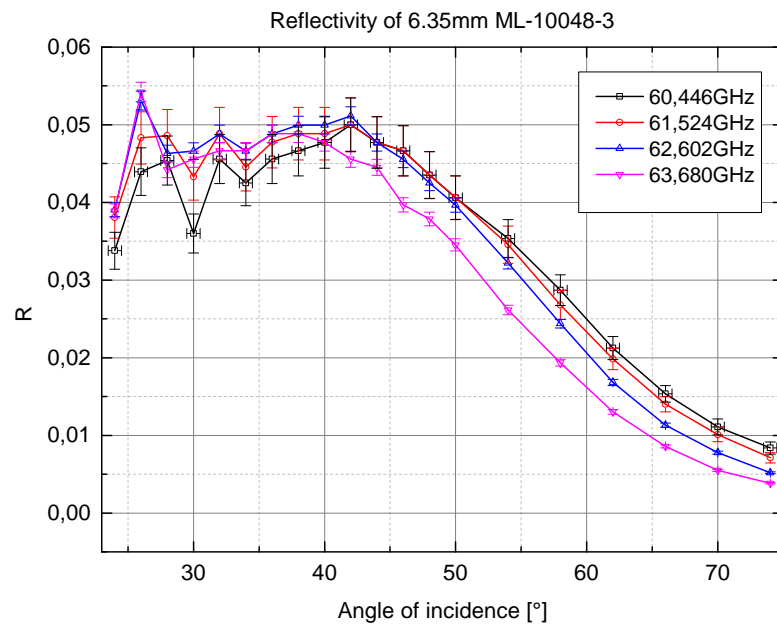
Looking at the reflectivity of 60.446 GHz in fig. 3.5(b), maxima are found at 42°, 32° and 28°. The expected values are a little smaller, but still in pretty good accordance, considering that there could have been variation in the foam's thickness. This supports the idea that interference causes the fluctuation in reflectivity at lower angles, because it follows an  $\arcsin(1/n)$  behaviour. However, from the data it can be inferred that the reflectivity of the material in the WR15 band will hardly exceed 7%, considering that the lower angle reflectivity in fig. 3.5 increases a little with the frequency and the WR15 band goes to 66 GHz in Europe. Reflections in the detector will mostly occur under higher angles at which the reflectivity averages about 1%.

---

<sup>1</sup>[www.arc-tech.com](http://www.arc-tech.com)



(a) 56 GHz to 60 GHz range



(b) 60 GHz to 64 GHz range

Figure 3.5.: Angular dependence of the reflectivity of graphite foam ARC ML-10048-3

Frequency [GHz]	Attenuation coefficient $\alpha$ [1/cm]	Loss [dB/cm]	$\chi^2_{red}$
56.134 ± 0.001	4.59 ± 0.31	19.93 ± 1.35	17.0
57.212 ± 0.001	4.70 ± 0.29	20.41 ± 1.26	16.0
58.290 ± 0.001	4.55 ± 0.30	19.76 ± 1.31	17.4
59.368 ± 0.001	4.72 ± 0.31	20.50 ± 1.35	19.1
60.446 ± 0.001	4.70 ± 0.32	20.41 ± 1.39	18.1
61.524 ± 0.001	4.80 ± 0.39	20.85 ± 1.70	25.0
62.602 ± 0.001	4.76 ± 0.33	20.67 ± 1.44	18.4
63.680 ± 0.001	4.80 ± 0.31	20.85 ± 1.35	18.2
average	4.70 ± 0.12	20.41 ± 0.53	

Table 3.1.: Loss and attenuation in graphite foam ARC LS-11451-1 with fit quality transmitting a 1 GHz sinusoid

The attenuation coefficient of the foam with model number LS-11451-1 (also from ARC Technologies) and the corresponding loss are displayed in table 3.1. The reduced  $\chi^2$ , i.e. the  $\chi^2$  divided by the number of degrees of freedom (2 in this case), is also given to estimate the quality of the fit from which the values were determined. Table 3.1 shows that these values are in the order of 20, meaning the fit is of poor quality, as  $\chi^2_{red}$  should ideally be one. It can be inferred that the absorption process in graphite foam for 60 GHz radiation doesn't exactly follow the Lambert-Beer law. However, the linearity observed in fig. 3.7, which shows an example fit, suggests it does so reasonably well and that instead the errors might be underestimated. For example, it was not investigated if the foam is homogeneous in its characteristics. The values obtained for the attenuation coefficient are thus to be understood as estimates. A graphic representation of table 3.1 is given in fig. 3.6.

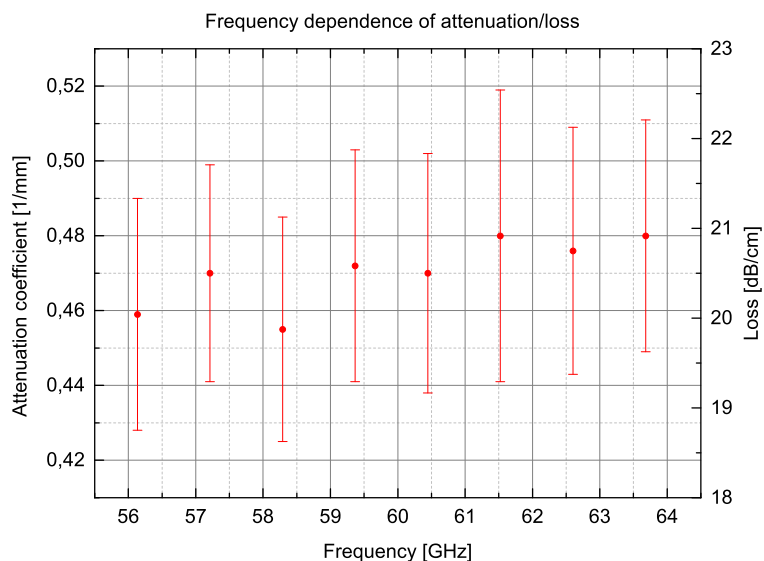


Figure 3.6.: Loss and attenuation in graphite foam ARC LS-11451-1 transmitting a 1 GHz sinusoid

As the errors outweigh any upward trend that could be identified from the diagram, it is reasonable to give an average attenuation coefficient for the frequency band. This value was found to be  $\alpha = (4.70 \pm 0.12) \text{ cm}^{-1}$ , corresponding to a loss of  $(20.41 \pm 0.53) \text{ dB/cm}$ .

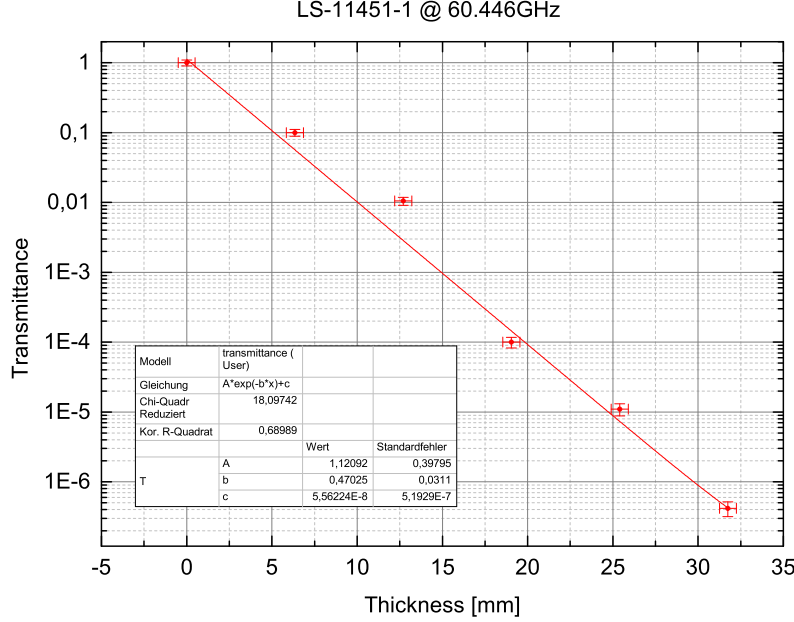


Figure 3.7.: Transmittance of graphite foam ARC LS-11451-1 at 60.446 GHz with exponential decay fit

The fit function used in fig. 3.7 and all other fits is eq. (3.3). While  $c$  was close to 0 for all fits, as it should be in the ideal case,  $A$  was systematically higher than 1, around 1.1 in all cases. This shows that part of the radiation is reflected. It is then

$$A \approx \frac{1}{1 - R} \quad (3.5)$$

$R$  being the reflectivity for perpendicular incidence, which allows for an estimate of the reflectivity; in this case it must have been around 10% in contrast to what was found for another foam in fig. 3.5.

Assuming the detector layers were coated entirely with 5 mm strength foam, upon incidence 2% of the radiation would be reflected directly (assuming the optimum values found with the reflectivity measurements rather than the estimated 10% of the other foam), the rest would be reflected completely by the silicon layer behind the foam [2]. Passing through more than 1 cm of foam effectively would result in a total reflectivity of just 3%. Further assuming a shielding that doesn't allow direct transmission for unwanted links (see fig. 3.2 again), at least 2 reflections would be necessary for cross-talk, only letting a fraction of 0.0009 of the radiation pass through. That would make cross-talk practically impossible, if the assumptions hold.

## 4. KAPTON FOIL GAIN HORN

All measurements described before were performed with a brass standard gain horn<sup>1</sup>. In a detector environment it is advantageous to employ materials of low atomic number to reduce multiple scattering and little material overall to reduce unwanted hadronic interactions. In an attempt to create a gain horn, that fulfills these requirements, aluminized Kapton®<sup>2</sup> foil (35 µm Kapton and 25 µm aluminum) was used to reproduce the brass antenna, i.e. to make an antenna of the same internal dimensions, which are displayed in fig. A.3. The heaviest atoms in Kapton are oxygen ( $Z=8$ ) and aluminum is the lightest metal ( $Z=13$ ). In combination with micrometer thickness this assures a low probability of multiple scattering or hadronic interactions. The approach was to create a negative of the brass antenna and then sheath it with the foil. The outcome is shown in figs. 4.1 and 4.2.

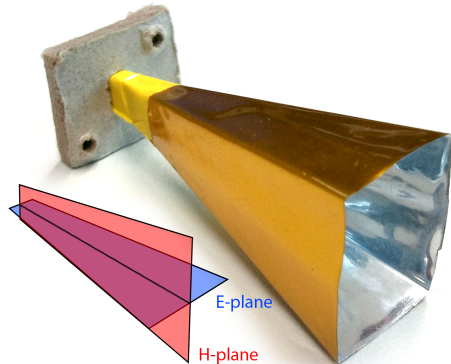


Figure 4.1.: Kapton antenna with position of planes



Figure 4.2.: Brass gain horn (left), negative (center), Kapton gain horn (right)

<sup>1</sup>Flann Standard Gain Horn Model-Nr. 25240-20 [27]

<sup>2</sup>polyimide film developed by DuPont™

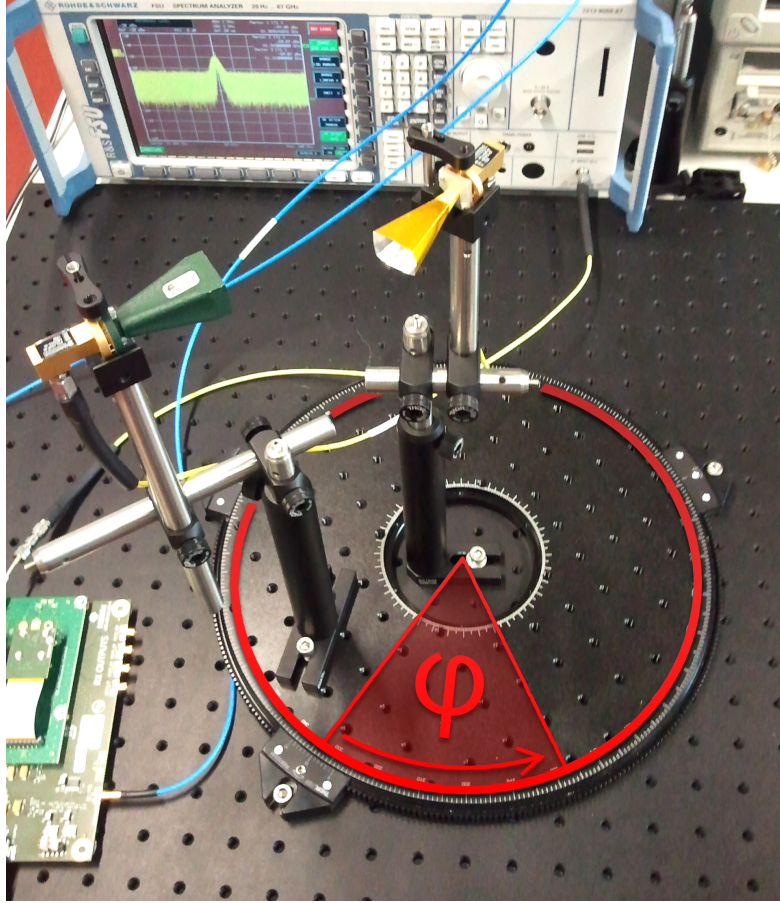


Figure 4.3.: Setup to determine the radiation pattern of the Kapton gain horn

## 4.1. EXPERIMENTAL SETUP

To quantify the directivity of the antenna it was placed in the central cut-out of a rotating breadboard onto which a brass gain horn was mounted, thus at a fix distance but under a variable angle. An illustration of the setup is given in fig. 4.3, which shows that not the antenna aperture but the waveguide opening was centered for this measurements. This way a comparison with the emission pattern of a waveguide is possible. One antenna was fed with a sine signal of intensity  $I_0$  and the transmitted intensity  $I_t$  was measured with a spectrum analyzer. The experiment was conducted for both the H-plane (long edge) and the E-plane (short edge) of the antenna (see fig. 4.1 again), where the names indicate the orthogonality of magnetic field and electric field, respectively. A detailed description of the influence of horn antennas on a propagating electromagnetic wave can be found in Jull [28], for example. A possible frequency dependence of the material's characteristics was also investigated. The results will be evaluated in the prospect of employing similar antennas within a detector.

## 4.2. MEASUREMENTS & RESULTS

For this section the emission characteristic of an aluminized Kapton foil gain horn was determined in order to investigate the feasibility of beam forming with micrometer strength materials of low atomic number. The setup is described in section 4.1. All measurements in this section were performed with a 1 GHz sine signal ( $-10 \text{ dBm}$  input power) fed to the baseband I input of the transceiver. The frequencies of the first lower and upper sidebands were thus at  $-1 \text{ GHz}$  and  $+1 \text{ GHz}$  with respect to the carrier frequency.

The maximum output power for different carriers, corrected for cable and connector losses, was measured by directly connecting the adapters used to supply the signal to the antennas, which is equivalent to 0 m transmission distance. The results are shown in table 4.1 and were used to give the antenna's emission characteristic in dBi rather than absolute measures.

Carrier frequency [GHz]	Lower sideband [dBm]	Upper sideband [dBm]
$57.134 \pm 0.003$	$-9.5 \pm 0.1$	$-6.9 \pm 0.1$
$58.212 \pm 0.003$	$-8.2 \pm 0.1$	$-10.2 \pm 0.1$
$59.290 \pm 0.003$	$-7.8 \pm 0.1$	$-12.2 \pm 0.1$
$60.368 \pm 0.003$	$-9.7 \pm 0.1$	$-12.5 \pm 0.1$
$61.446 \pm 0.003$	$-11.1 \pm 0.1$	$-13.8 \pm 0.1$
$62.524 \pm 0.003$	$-10.8 \pm 0.1$	$-15.1 \pm 0.1$
$63.602 \pm 0.003$	$-11.4 \pm 0.1$	$-17.1 \pm 0.1$
$64.680 \pm 0.003$	$-11.5 \pm 0.1$	$-17.3 \pm 0.1$

Table 4.1.: Maximum intensity (corresponding to 0 m transmission distance) transmitting a 1 GHz sinusoid

The set was also used to investigate the frequency dependence of the forward gain. An increase with the frequency similar to that of the brass gain horns (see fig. 4.4) was expected but not observed. Instead the gain values varied between 13 dBi and 18 dBi as seen in fig. 4.5.

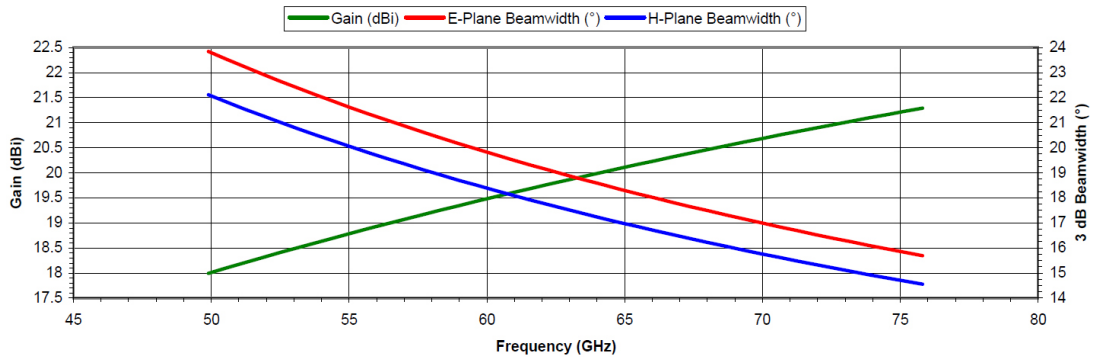


Figure 4.4.: Performance data of the brass gain horns [27]

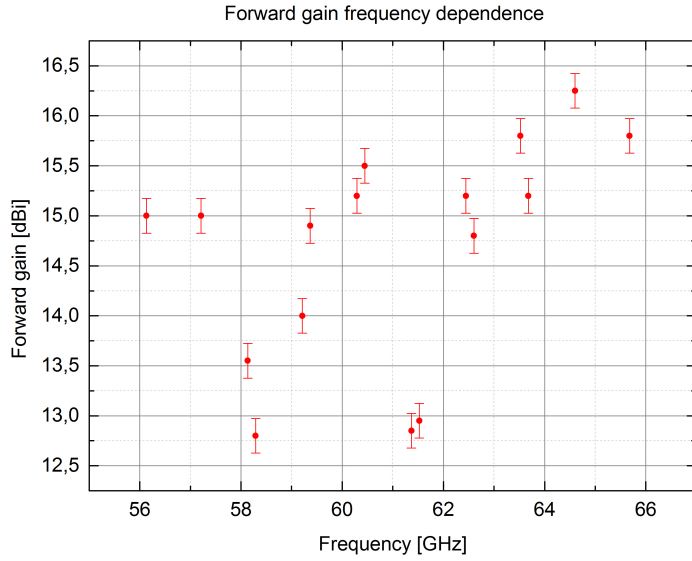


Figure 4.5.: Kapton gain horn forward gain

It was observed that values were very susceptible even to minor changes of the antenna, which itself is rather fragile. Hence every mounting and unmounting resulted in hardly compensable changes to the antenna. In addition to that the emission pattern of gain horns is strongly frequency dependent. Imperfections in the antenna's form could have caused the maximum intensity to be shifted away from  $0^\circ$  for the frequencies around 58 GHz and 62 GHz. The asymmetric patterns seen in figs. 4.6 and 4.7 support this explanation.

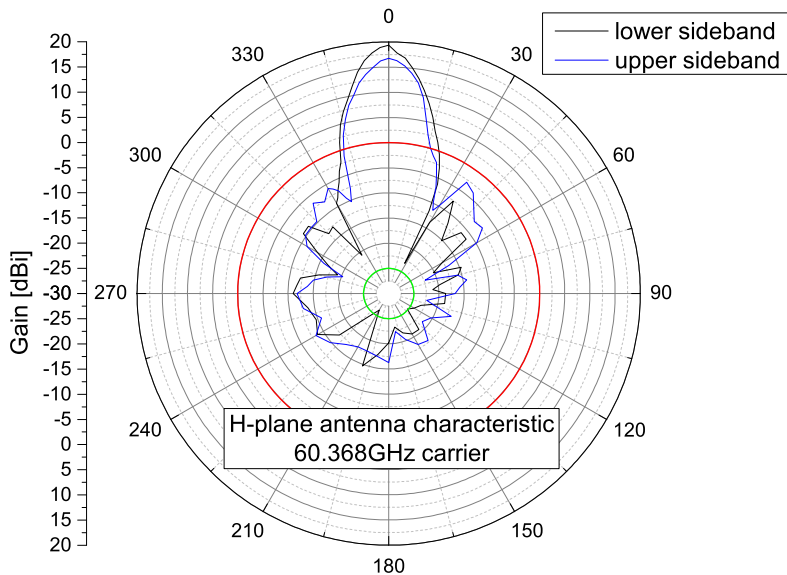


Figure 4.6.: H-plane characteristic of the Kapton foil gain horn transmitting a 1 GHz sinusoid; isotropic emitter (red); noise (green)

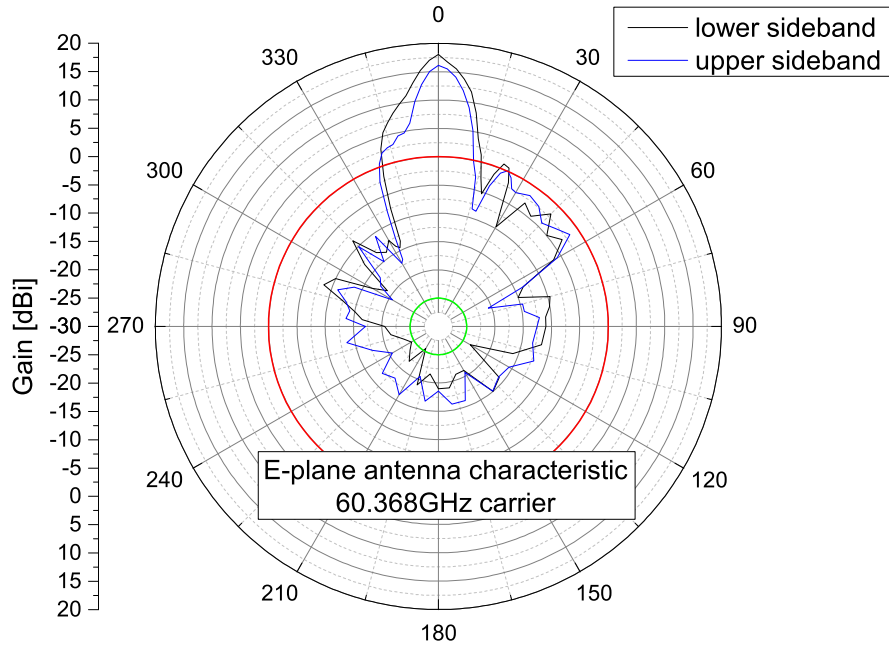


Figure 4.7.: E-plane characteristic of the Kapton foil gain horn transmitting a 1 GHz sinusoid; isotropic emitter (red); noise (green)

The emission pattern of the Kapton gain horn for both H- and E-plane are displayed in figs. 4.6 and 4.7 and the levels of noise and an isotropic emitter are given for comparison. It is clearly visible that a directivity comparable to that of more sophisticated antennas can be achieved. An ideal 3D radiation pattern is shown in fig. A.4 and the emission pattern of a waveguide aperture is displayed in fig. 4.8. The Kapton antenna presents the characteristic forward "bulb", but other sidelobes cannot be seen. Instead, noise-like emission, but of higher intensity than the background indicated by the green line, is seen between 30° and 330°. This distortion is likely a result of imperfections in the connection between the antenna and the adapter to coaxial cable. In this case, the antenna mounting was facilitated by simple cardboard, as seen in fig. 4.1, and hence error-prone. While not sufficient for quantitative measurements, a qualitative analysis was intended and indeed possible with this rather primitive prototype.

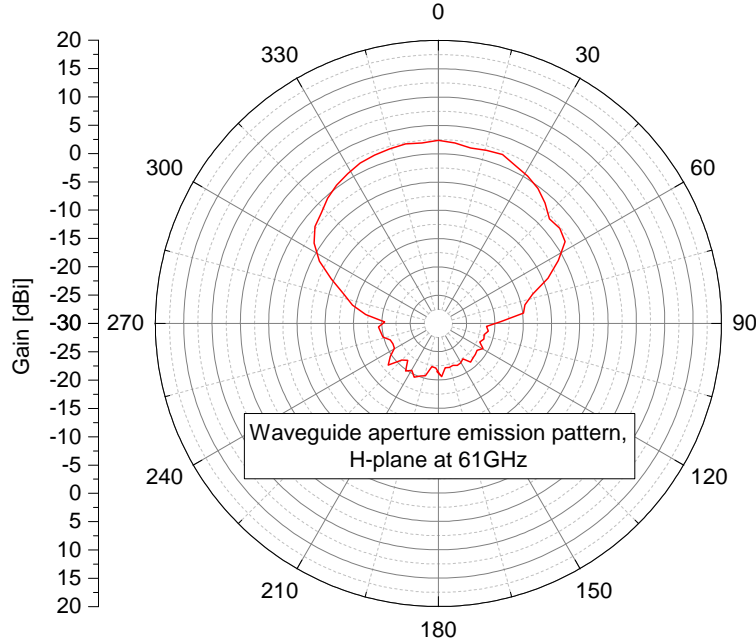
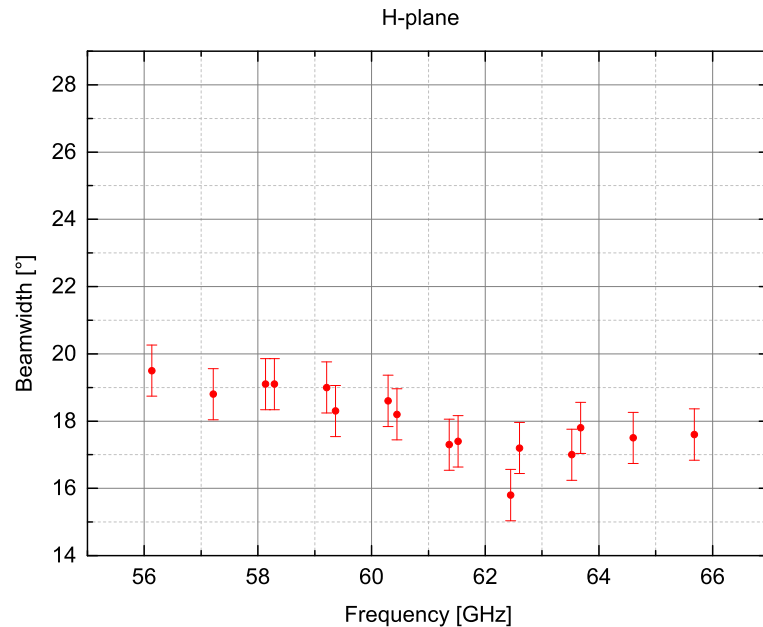
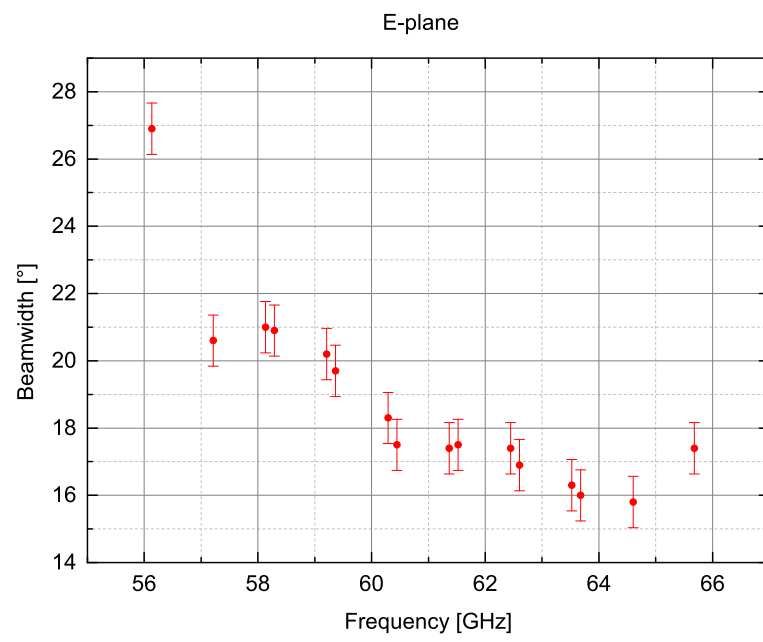


Figure 4.8.: Emission pattern of a waveguide aperture transmitting a 1 GHz sinusoid [29]

The half maximum ( $-3\text{ dB}$ ) beamwidth was measured and can be seen in fig. 4.9. For both planes a small decrease with increasing frequency is visible, more pronounced for the E-plane. This was expected from the performance data of the brass gain horns (see fig. 4.4 again). The first data point recorded for the E-plane appears to be outside of reasonable range, but the measurements were highly susceptible to minor changes of the antenna's form and although all adjustments were performed carefully, the horn's fragile structure remains an error source. The given errors do not account for such systematic flaws. However, the beamwidth is of the same order as that of the brass gain horn - around  $20^\circ$  - indicating that beamforming can be achieved with the examined material, which would greatly reduce cross-talk between neighbouring data links.



(a) H-plane beamwidth



(b) E-plane beamwidth

Figure 4.9.:  $-3$  dB beamwidth of the Kapton foil gain horn transmitting a 1 GHz sinusoid

## 5. DISCUSSION

For the first part of this work, the performance of a full 60 GHz transceiver evaluation kit (in short referred to by the developing company's name Hittite) was investigated in order to establish a testbench for future systems. The input and output signal quality for digital signals was compared and bit error rates were measured for short time spans. The phase of the output was analyzed and reasons for an instability thereof were given. The RF spectrum was recorded for both internal and external clock supply. Another transceiver chipset (Gotmic) was briefly introduced for comparison.

The attempt to establish stable data transmission via simple IQ baseband modulation and measure the bit error rate for different data rates was successful only for shorter periods of time, returning BER between  $10^{-9}$  and  $10^{-11}$ . If it had been possible to keep the transmission stable for longer times, error rates orders below these values would've likely been observed. Output phase instability and distortions in signals with high frequency content were identified as the main error sources. The input signal for the BER measurements was also analyzed and found to be very clean, thus not likely to cause errors.

Analyzing the phase of both Q and I output with respect to a sine input on I showed that neither output is necessarily in phase with the input. Some phase offset is of course expected due to the difference in runtime, but that offset would be constant. Neglecting such offset, the outputs were found in a seemingly random manner at multiples of  $90^\circ$  relative to the input when transmitting a 1 GHz sine signal, changing every time the transmitter or the receiver was reset. This effect is most likely caused by the transmitter and the receiver PLLs locking on different points of the input clock. In addition to the arbitrary difference of multiples of  $90^\circ$ , a phase drift was observed, which could be explained by an unstable input clock. However, no comprehensive explanation for the random phase between the two outputs can be made without knowing the exact design of the circuitry responsible for the demodulation. For the transmission of a 150 MHz sine the random reset wasn't observed, instead the phase of both outputs was highly unstable. The difference could be that the latter is less than half of the clock frequency while 1 GHz is more than twice the clock frequency and hence enough to make the phase difference between transmitter and receiver clock fully visible. The phase instability would not be an issue if a modulation had been chosen that doesn't require coherent demodulation. Clock distribution with a stable phase could be a potential challenge for a wireless detector readout, so it might be advantageous to resort to simpler modulation such as OOK or FSK, especially since bandwidth is not expected to be a bottleneck, as described in section 2.1.4. However, for the gotmic transceiver chipset, which has a simpler design than the Hittite one, the phase instability was not observed - although verified only for frequencies  $< 200$  MHz - indicating that coherent demodulation should not be disqualified completely.

It was found that neither with the use of an internal oscillator nor with an external clock the RF spectrum of the Hittite transmitter featured undisturbed frequency peaks,

a requirement for clean demodulation as shown in section 2.1.4. While an instability of the internal quartz oscillator can explain the deviation of the analyzed peak, the external clock supply was indeed very stable, indicating that the connection between the clock input and the multiplier stage might be defective. From the clean shape of the peaks in the transmission spectrum when using the internal oscillator it can be inferred that the multiplier itself was most likely working correctly. Another likely cause of the distortion could be frequency content picked up by the setup through cables or otherwise that was then fed into the multiplier along with the desired clock frequency. An attempt to shield the setup with aluminum foil failed as it did not observably affect the situation. It would have been desirable to be able to probe the isolated multiplier module and the clock input to further pinpoint the source of the observed frequency distortion. More frequency stability would most likely lead to an improved transmission quality and the unstable clock supply could well have caused all other observed issues.

The second part of this work aimed to investigate, if graphite foam could be used as an absorber for 60 GHz radiation and if aluminized kapton foil could be used in form of a gain horn for beam forming. Both materials offer a low atomic number to prevent multiple scattering and low mass to prevent hadronic interactions. For the foam both reflectivity and attenuation were measured.

The analysis of two different types of graphite foam showed that a reflectivity lower than 2% for angles of incidence between 70° and 90° and an average transmission loss of 20 dB/cm can be achieved, which should be enough to reliably prevent cross-talk issues. It was also observed that the frequency dependence of both the reflectivity and the attenuation within the WR15 band are rather small. For future estimations or simulations it will be sufficient to work with average values for the frequency band.

The very low atomic mass and density ( $32 \text{ kg/m}^3$  [22]) of the foam will result in low multiple scattering and the high performance observed in the experiment make it reasonable to employ such foam for cross-talk suppression. As mentioned in section 3.2, as little as 5 mm covering the detector's silicon layers can suffice to fulfill that purpose. If a wireless readout is to be implemented, a detailed analysis of different foams should be performed to find the material with the best performance and best suitable for the use inside a particle detector. Flexibility, for example, might be a desirable quality.

It was found that with a gain horn made from aluminized kapton foil a directivity comparable to metal cast gain horns can be achieved. The  $-3 \text{ dB}$  beamwidth was found to be around 20° for the dimensions given in fig. A.3. Considering that such antennas would hardly strain a detector's material budget and neither increase the likelihood of multiple scattering/hadron interactions, the use of aluminized Kapton foil for beam-forming purposes is reasonable. With a length of 4.8 cm the current prototype is likely oversized with respect to the limitations posed by the detector geometry. Some directivity and gain would have to be traded off against more desirable dimensions. If the use of Kapton gain horns is required, a more extensive analysis would be recommendable to find an optimized combination of size and performance. While the detector itself limits dimensions on the higher end, the wavelength of  $\sim 5 \text{ mm}$  does so on the lower end. As seen in figs. 4.6 and 4.7 a clean connection between the antenna and the waveguide is mandatory to keep power loss to a minimum.

# ACKNOWLEDGEMENTS

First and foremost I would like to thank Prof. André Schöning for giving me the opportunity to carry out this thesis and for his support throughout the whole process. I would also like to thank the whole group for providing an excellent working environment.

For guidance, assistance and ongoing support in various matters I wish to express gratitude towards Dr. Dirk Wiedner, Dr. Niklaus Berger and Hans Kristian Soltveit, who invested a lot of time and effort to help me finish this work. Christian Färber and Sebastian Dittmeier were also very supportive and lent me a helping hand on numerous occasions.

Dr. Johannes Schemmel kindly agreed to function as second examiner for this thesis, for which I would like to thank him.

# REFERENCES

- [1] *HL-LHC: High Luminosity Large Hadron Collider*. Online. Apr. 2013. URL: <http://hilumilhc.web.cern.ch/hilumilhc/index.html>.
- [2] Richard Brenner and S. Cheng. “Multigigabit wireless transfer of trigger data through millimetre wave technology”. In: *Workshop on Intelligent Trackers 2010*. Lawrence Berkeley National Lab, Feb. 2010.
- [3] H.K. Soltveit et al. “Multi-Gigabit Wireless data transfer at 60 GHz”. In: *Workshop on Intelligent Trackers 2012*. INFN Pisa, May 2012.
- [4] E. Lipeles. “L1 track triggers for ATLAS in the HL-LHC”. In: *Topical Workshop on Electronics for Particle Physics 2011*. Vienna, Austria, Sept. 2011.
- [5] *ATLAS Fact Sheet*. CERN. Mar. 2013. URL: [http://www.atlas.ch/pdf/atlas\\_factsheet\\_all.pdf](http://www.atlas.ch/pdf/atlas_factsheet_all.pdf).
- [6] P.J. Dervan. “Silicon strip detectors for the ATLAS HL-LHC upgrade”. In: *9th International Conference on Position Sensitive Detectors*. Aberystwyth, U.K., Sept. 2011.
- [7] *60 GHz frequency band*. Online. Apr. 2013. URL: <http://www.itwissen.info/definition/lexikon/60-GHz-Band-60-Ghz-frequency-band.html>.
- [8] *Wireless HD: The First 60 GHz Standard*. Online. Apr. 2013. URL: <http://www.wirelesshd.org/>.
- [9] M. Goresky and A.M. Klapper. “Fibonacci and Galois representations of feedback-with-carry shift registers”. In: *IEEE Transactions on Information Theory* 48.11 (Nov. 2002), pp. 2826–2836.
- [10] *TXQ060A01 60GHz transmitter*. Gotmic AB. Apr. 2013. URL: <http://gotmic.se/documents/TXQ060A01.pdf>.
- [11] *RXQ060A01 60GHz receiver*. Gotmic AB. Apr. 2013. URL: <http://gotmic.se/documents/RXQ060A01.pdf>.
- [12] *HMC6000 Millimeterwave Transmitter IC*. Hittite Microwave Co. Apr. 2013. URL: <http://www.hittite.com/products/view.html/view/HMC6000>.
- [13] *HMC6001 Millimeterwave Receiver IC*. Hittite Microwave Co. Apr. 2013. URL: <http://www.hittite.com/products/view.html/view/HMC6001>.
- [14] Roger L. Freeman. *Radio System Design for Telecommunication*. 3rd ed. Wiley, Aug. 2007.
- [15] S. Pasupathy. “Minimum shift keying: A spectrally efficient modulation”. In: *Communications Magazine, IEEE* 17.4 (July 1979), pp. 14–22.
- [16] Martin Werner. *Nachrichtentechnik. Eine Einführung für alle Studiengänge*. 7th ed. Springer, 2010, pp. 120–121.

- 
- [17] Ulrich Schmidt. *Professionelle Videotechnik*. 4th ed. Springer, 2005, pp. 224–225.
  - [18] Altera Corporation. *The Evolution of High-Speed Transceiver Technology*. White Paper. Nov. 2002. URL: [http://www.altera.com/literature/wp/wp\\_hs\\_transceiver.pdf](http://www.altera.com/literature/wp/wp_hs_transceiver.pdf).
  - [19] Stefan Swientek. “A fast Backend readout for the LHCb Outer Tracker Upgrade”. In progress. PhD Thesis. TU Dortmund.
  - [20] Thomas Hugle. “Simulation von Datenübertragung und Beugung mit einem Ray-tracer”. BSc Thesis. University of Heidelberg, 2013.
  - [21] Robert Felbecker et al. “Estimation of Effective Permittivity and Effective Thickness of Inhomogeneous Materials at 52 – 70 GHz”. In: *3rd European Conference on Antennas and Propagation (EuCAP 2009)*. Berlin, Germany, Mar. 2009.
  - [22] *Microwave Absorbing Materials*. Telemeter Electronic. Apr. 2013. URL: [http://www.telemeter.info/documents/absorbing\\_materials.pdf](http://www.telemeter.info/documents/absorbing_materials.pdf).
  - [23] David R. Vizard. “Millimeter-wave Applications: From Satellite Communications to Security Systems”. In: *Microwave Journal* (July 2006).
  - [24] Wolfgang Demtröder. *Experimentalphysik 2. Elektrizität und Optik*. Springer, 2004, p. 221.
  - [25] Eugene Hecht. *Optik*. 4th ed. Oldenbourg, 2005, pp. 192–207.
  - [26] William Lawrence Bragg. “The diffraction of Short Electromagnetic Waves by a Crystal”. In: *Proceedings of the Cambridge Philosophical Society*. 1913, pp. 43–57.
  - [27] *Standard Gain Horn Model 25240-20*. Flann Microwave Ltd. Mar. 2013. URL: <http://www.flann.com>.
  - [28] Edward V. Jull. *Aperture Antennas and Diffraction Theory*. Peter Peregrinus Ltd. for IEE, 1981.
  - [29] Sebastian Dittmaier. “Wireless detector readout at 60 GHz”. In progress. MSc thesis. University of Heidelberg, 2013.

## A. APPENDIX

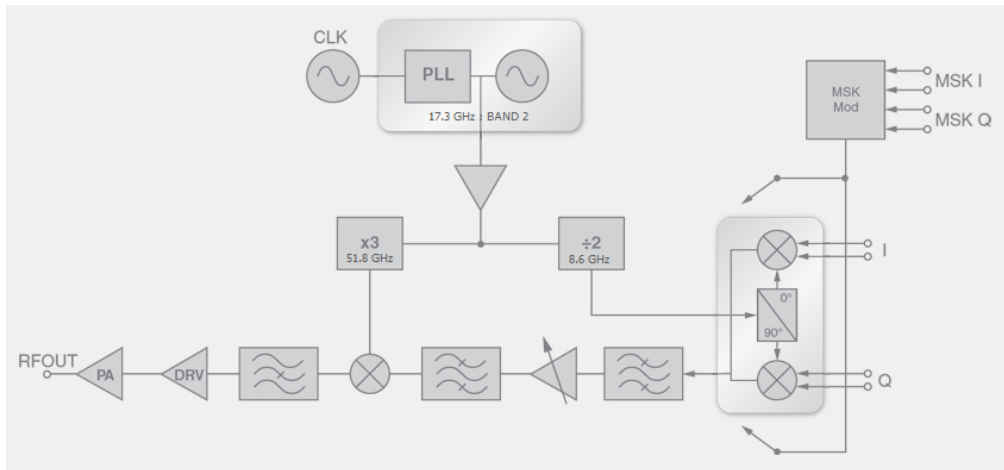


Figure A.1.: Transceiver Evaluation Kit Transmitter Layout (taken from the control software)

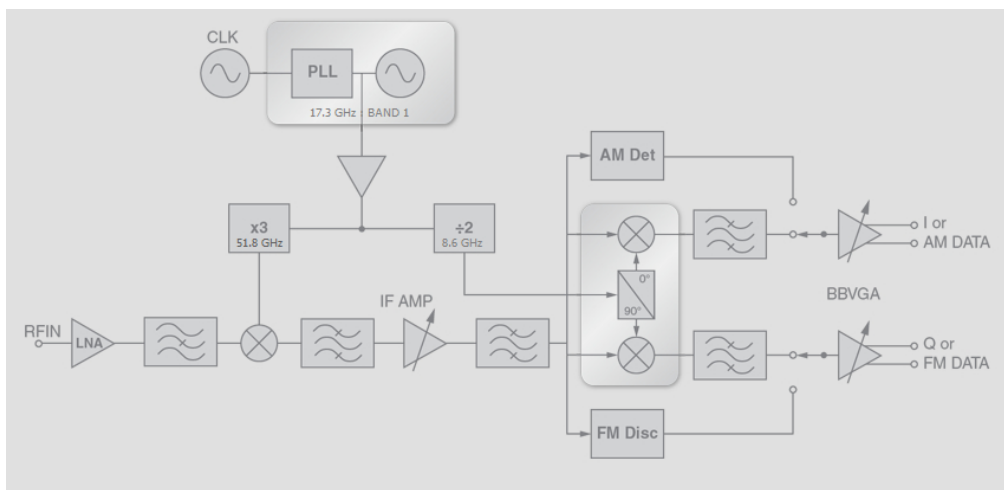


Figure A.2.: Transceiver Evaluation Kit Receiver Layout (taken from the control software)



## Standard Gain Horn

Model 25240-20

Waveguide Size:  
Nominal Gain:  
Operating Frequencies:

WG25 (WR15, R620)  
20 dBi  
49.9 - 75.8 GHz

Overall Length (A):  
Aperture Width (B):  
Aperture Height (C):  
Waveguide Width (D):  
Waveguide Height (E):  
Flare Length (F):

48.0 mm (1.890 inch)  
18.50 mm (0.728 inch)  
12.80 mm (0.504 inch)  
3.759 mm (0.148 inch)  
1.880 mm (0.074 inch)  
38.00 mm (1.496 inch)

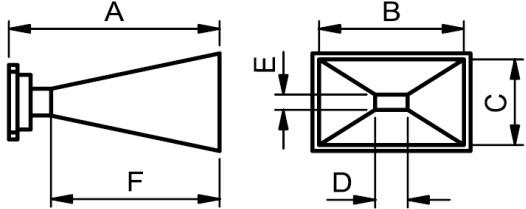


Figure A.3.: Dimensions of the gain horns in use. H-plane is parallel to B, E-plane is parallel to C [27]

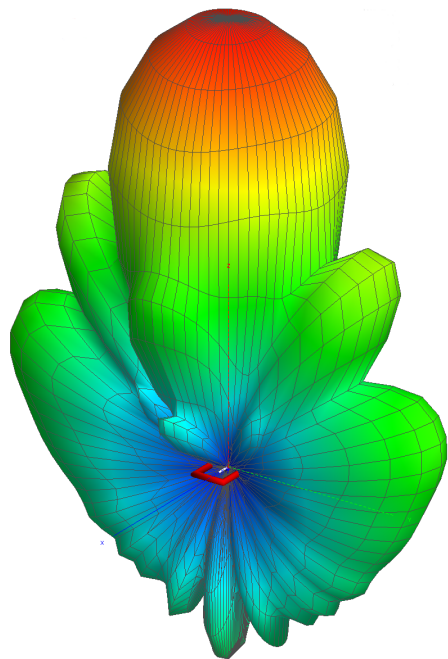


Figure A.4.: Ideal emission pattern of the gain horn used in the experiment [29]

# DECLARATION

I hereby declare that this thesis is my own work and effort. It has not been submitted elsewhere for any award. I have not used any source of information other than those acknowledged.

Heidelberg, 30th of April 2013

.....